https://doi.org/10.5194/wes-2026-63
Preprint. Discussion started: 9 April 2026

eawe european academy of wind energy
Open Access WIND ENERGY SCIENCE DISCUSSIONS

Case study of a site-specific design and operation optimization of a wind farm co-located PEM electrolyzer and BESS including degradation

Dustin Frings[1], Georg Jacobs[1], Thorsten Reichartz[1], Thora Potthoff[1], Lucas Blickwedel[1], and Martin Knops[1]

[1]Chair for Wind Power Drives, RWTH Aachen University, Aachen, 52074, Germany

Correspondence to: Dustin Frings (dustin.frings@cwd.rwth-aachen.com)

Abstract. The expansion of volatile renewable energy sources leads to increased electricity price volatility and cannibalization effects, intensifying the economic pressure on project developers. Decentralized hybrid energy systems for renewable hydrogen production offer a solution to exploit these price fluctuations and counteract curtailment during hours of low or negative electricity prices. However, the design and operation of those systems are inherently coupled and significantly influenced by external factors, such as electricity and hydrogen prices that can be achieved over the lifetime. To determine an economically optimal design, specifically the power of an electrolyzers and the capacity of a battery, both site-specific and plant-specific characteristics must be considered.

First, this paper presents a methodology for determining the optimal electrolyzer rated power and lithium-ion buffer battery capacity size for a 68 MW wind farm in north-western Germany. The approach extends an existing site-specific design method by introducing a battery storage system and enhancing the electrolyzer model with part-load efficiency and operating-mode-dependent degradation. Results indicate that neglecting degradation leads to an underestimation of the levelized cost of hydrogen (LCOH) by 1.2 € kg^{-1}, corresponding 21 %, while neglecting both degradation and part-load efficiency increases this underestimation to 35%. Concurrently, the inclusion of the battery energy storage system (BESS) can reduce electrolyzer degradation by more than one-third and increase the annual operational profit by 5 %, while it leads to a marginal LCOH increase of 1 % due to higher capital expenditures. For the design phase, a price-independent operational strategy aiming to maximizing renewable hydrogen yield was implemented, representing a necessary simplification.

This operational assumption within the design phase was validated in a second step through a mixed-integer linear (MIL) operational optimization. This assessment reveals two key findings: Firstly, the assumption of a constant archivable electricity price over the systems lifetime leads to a 23 % overestimation of annual operational profits when compared to the more realistic electricity sales at the German day-ahead market in 2024. Secondly, the operation heuristic of the design method demonstrates high economic competitiveness, deviating by only 4.5 % from the theoretical MIL optimum even under reduced hydrogen pricing. Nevertheless, this performance may be site-specific, as integrated optimization may yield significantly higher added

https://doi.org/10.5194/wes-2026-63
Preprint. Discussion started: 9 April 2026

eawe european academy of wind energy
Open Access WIND ENERGY SCIENCE DISCUSSIONS

value in markets characterized by greater price volatility or different meteorological profiles. Beyond these specific results, the model showcases the critical importance of integrating high-fidelity physical effects for electrolyzer models, alongside the strategic inclusion of battery storage. Furthermore, it demonstrates that a rigorous consideration of the operational strategy is necessary for a robust and reliable system assessment to account for volatile external factors. Overall, the proposed method provides wind farm developers with a tool to evaluate and optimize site-specific wind-hydrogen-battery systems to derive well-founded strategic investment decisions.

1 Introduction

To achieve the European Union's climate target of reducing greenhouse gas emissions by 55 % by 2030 (European Parliament and Council 2021), the share of renewable energy in the energy mix is planned to be increased to 42.5 % and the production of 10 million tons of green hydrogen is targeted by 2030 (European Comission 2026). However, the rapid expansion of renewable energies and its volatile electricity generation pose significant challenges for grid and wind farm (WF) operators, including curtailment and declining revenues from electricity sales. Besides grid-induced curtailments, cost-induced curtailment of WFs during hours of negative electricity prices reduces the utilization of available wind resources. Meanwhile, WF operators encounter revenue declines due to prize cannibalization and high price volatility (Bechmann und Quick 2025). Concurrently, the marginal cost of wind power production has already attained a relatively low level (Bošnjaković et al. 2022), with no further drastic cost reductions expected. These effects increase pressure on WF operators, forcing them to consider new revenue streams and operation concepts. One way to counter these problems are hybrid renewable energy systems (HRES) consisting for example of a WF, a solar photovoltaic (PV) system, a battery energy storage system, and an electrolyzer to produce green hydrogen (Canbulat et al. 2021). The economic viability of such integrated systems is increasingly supported by the rapid decline in capital expenditures for key components. In particular, the cost of utility-scale battery storages has decreased by over 80 % in the last decade (IRENA 2024), enabling HRES configurations that were previously economically unfeasible. From an economic perspective, HRES can temporarily decouple renewable electricity generation from electricity sales, enabling a more efficient utilization of available wind resources, as wind power generation can continue during grid- or price-induced curtailment events. Additionally, HRES potentially offer ancillary services like secondary control reserve, voltage control, or black start capability (Robinius et al. 2017; van Phan et al. 2024; Cozzolino and Bella 2024). From a business perspective electricity generated during hours with low or negative electricity prices can be stored in BESS, sold later or converted into hydrogen. However, the additional flexibility in the operation of the HRES makes the operation and thus its optimal techno-economic design complex (Rozzi et al. 2025), as the operation moves beyond a simple wind-to-grid connection to encompass multiple, multi-directional power flows between the WF, the grid, the BESS, and the electrolyzer.

Various studies investigate the design of different types of HRES. Schnuelle et al. (2020), Hofrichter et al. (2023), Fabianek und Madlener (2024), Grant et al. (2024), and Tezer (2025) eighter evaluated given systems without optimizing the components

https://doi.org/10.5194/wes-2026-63
Preprint. Discussion started: 9 April 2026

design or they lack on detail by only focusing on the main components of their considered HRES, neglecting the influence of site-specific conditions or sub-systems such as hydrogen storage, pipelines, compressor or equipment for the electrolyzer power supply. These aspects are considered within the design methodology introduced by Reichartz et al. (2024a), that minimizes the levelized cost of hydrogen (LCOH) for a WF-electrolyzer system. Giving the hourly WF power output over one year they optimize the electrolyzer design and the position of all components including the point of water supply and different distribution modes like a hydrogen pipeline or storage combined with trailers. They used a highly simplified electrolyzer model with constant efficiency and without degradation effects. However, the operation of an electrolyzer strongly influences its degradation and therefore its efficiency loss (Papakonstantinou et al. 2020; Zheng et al. 2023; Sayed-Ahmed et al. 2024). Consequently, the proposed methodology underestimates maintenance and replacement costs and, therefore, the LCOH. Ibáñez-Rioja et al. (2025) minimize LCOH, model degradation, and component replacement for a WF, PV, water electrolyzer, hydrogen storage, and BESS. However, their case relies on assumptions regarding the demand side, specifically by assuming constant hydrogen demand and off-grid operation. Additionally, they used geological hydrogen storage that is highly location dependent. All the mentioned studies on HRES design methodologies minimize LCOH, however, this keeps focus on reducing hydrogen system costs while maximizing the annual hydrogen product (AHP), although HRES operators aim to maximize the profit of the overall HRES. Accurately calculating this profitability requires an estimation of potential revenues, which in turn necessitates an approximation of the system's operation. To model this operation behavior of the systems components within the design stage a predefined operation strategies can be utilized, meaning it is initially defined at what time electricity is fed into an electrolyzer, a battery, or if considered the electricity grid (Hofrichter et al. 2023; Grant et al. 2024; Tezer 2025). However, this can lead to a suboptimal design compared to the actual system behavior under varying price conditions leading to potential over- or underestimated revenues and costs (Kansara und Roldán Serrano 2024; Zheng et al. 2022). To overcome the issue of a determined operating strategy, two-stage optimization consisting of an outer design optimization and an inner operation optimization loop are utilized (Balderrama et al. 2019; Dolatabadi et al. 2019; Zheng et al. 2022; Shams et al. 2021). These approaches, however, ignore either part-load efficiency, degradation of the electrolyzer, or site-specific cost conditions. Moreover, some do not include a BESS, even though battery integration can enhance the HRES revenue potential and mitigate electrolyzer degradation (Peng et al. 2025; Nachit et al. 2026).

While existing literature frequently investigates HRES design, many studies rely on simplified electrolyzer models or overlook site-specific infrastructure. Furthermore, the prevailing focus on LCOH minimization and fixed operating strategies often neglects the potential for profit maximization and the strategic synergies of battery integration in volatile market conditions.
In this study, the observed HRES consists of a WF, a proton exchange membrane (PEM) electrolyzer, and a BESS as main components, as well as additional subcomponents consisting of a power cable, power converter, water pipe, water pump, hydrogen pipe, hydrogen compressor, and hydrogen storage. We assume an existing WF and first optimize the design of the electrolyzers rated power and the BESS capacity to achieve the maximum annual profit (AP). Since all components will be placed close to an already existing WF we will further call the considered HRES a hybrid wind farm (HWF). Following the

https://doi.org/10.5194/wes-2026-63
Preprint. Discussion started: 9 April 2026

eawe european academy of wind energy
Open Access WIND ENERGY SCIENCE DISCUSSIONS

approach of Hofrichter et al. (2023), the design phase to optimize the rated electrolyzer power and BESS capacity employs an operation strategy that defines power flows for all design components. This methodology entails assumptions regarding system operation that are evaluated by a subsequent mixed-integer linear (MIL) operation optimization for the optimized HWF design. This is done over a historical year by maximizing the operational annual profit (OAP) focussing explicitly on the operational revenues and costs. The MIL operation optimization includes a time constant and linearized part-load efficiency of the electrolyzer. This is a simplification that will be validated by a subsequent evaluation of the electrolyzer degradation and the linearized part-load efficiency to determine the more realistic OAP. Thus, this work provides guidance for decision makers in identifying an optimal HWF design and an optimized operation with electrolyzer degradation effects by answering the following research questions:

- For a given WF, what is the optimum PEM electrolyzer rated power and BESS capacity for maximum annual profit taking site-specific costs, electrolyzer part-load efficiency, and degradation into account, while assuming a fixed operating strategy for the hybrid wind farm design components?
- How does the integration of a BESS and the consideration of electrolyzer degradation and part-load efficiency influence the LCOH of the HRES?
- To what extent can a MIL operation optimization and a subsequent degradation evaluation increase the operational annual profit compared to the design method?

To answer these questions, in Sect. 2 the methodology for the design optimization, the MIL operation optimization and the degradation evaluation with all underlying assumptions is described. Section 3 introduces a case study of which the methodology is applied and results are presented. In Sect. 4 results and limitations of the presented methodology are discussed and further research needs are indicated.

2 Methodology

The following section describes the fundamentals for understanding the extended design optimization (Sect. 2.2), that is based on the method of Reichartz et al. (2024b). The design method is extended by a more detailed electrolyzer model as described in Sect. 2.1 and the objective to maximize the AP instead of minimizing LCOH. A subsequent MIL operation optimization to evaluate the operation strategy assumed in the design optimization is described in Sect. 2.3. Figure 1 presents the overall methodology with all respective optimization and evaluation steps, inputs, parameters, optimization variables, and outputs.

https://doi.org/10.5194/wes-2026-63
Preprint. Discussion started: 9 April 2026

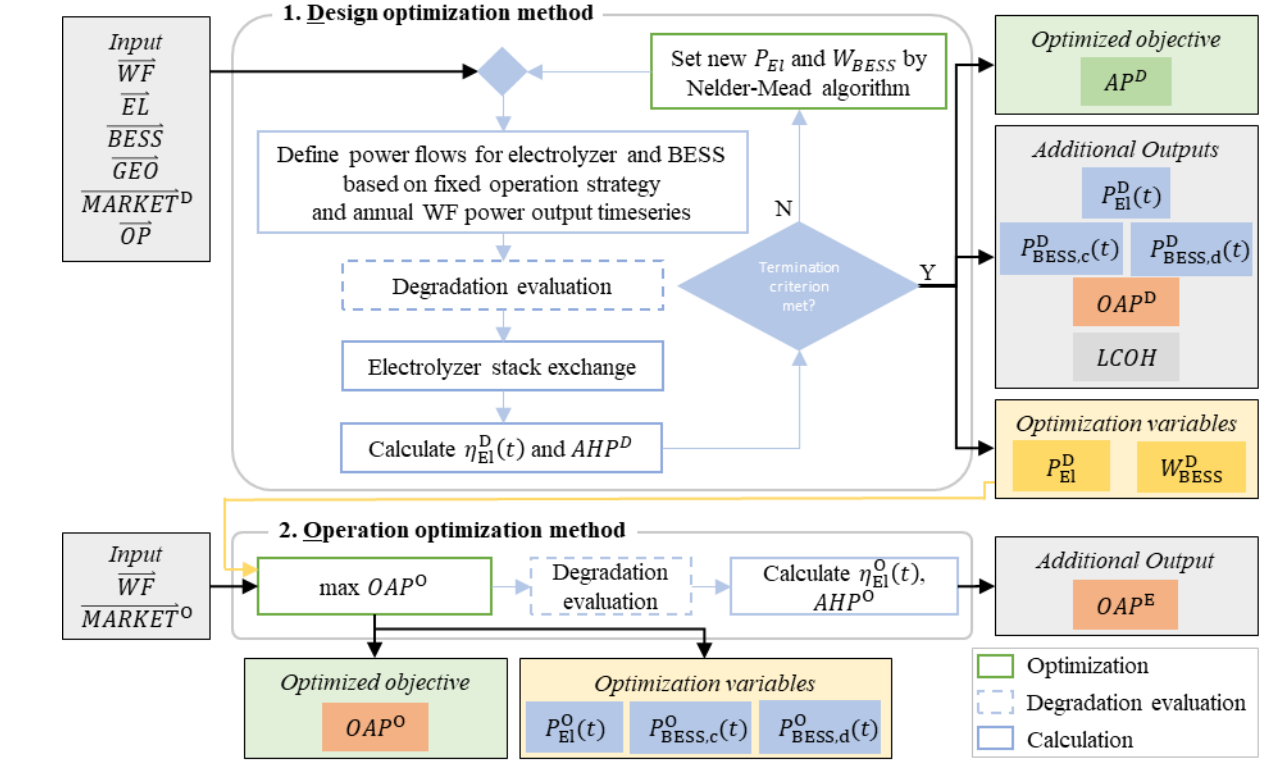

Figure 1: Schematic overview of the proposed design methodology (superscript index D) and the subsequent MIL operation optimization (superscript index O).

Bevor starting the design optimization input parameters need to be defined. The method described by Roscher (2020) is used to calculate the necessary WF input parameter vector $\overrightarrow{\boldsymbol{WF}}$. Based on an existing WF with a given nominal capacity P_{WF}, a site, weather data from the New European Wind Atlas (2026), the expected LCOE and a hourly time series of the WF power output $P_{\mathrm{WF}}(t)$ for a chosen weather year is calculated. The electrolyzer input parameter vector $\overrightarrow{\boldsymbol{EL}}$ depends on the electrolyzer technology and consists of an initially set electrolyzer rated power P_{El} and BESS capacity W_{BESS}. It also contains the power ratio at which we assume the electrolyzer to operate in rated power mode $P_{\mathrm{El,rated}}^{\mathrm{min}}\ P_{\mathrm{El}}{}^{-1}$, the rated power P_{Stack} and the minimum part load $P_{\mathrm{Stack}}^{\mathrm{min}}$ of a single electrolyzer stack. Electrolyzer cell related parameters are the maximum current density $i_{\mathrm{cell}}^{\mathrm{max}}$, the maximum cell voltage $U_{\mathrm{cell}}^{\mathrm{max}}$, the cell area A_{cell}, the operating temperature T_{cell}, the operating pressure p_{H_2} and p_{O_2}, the transfer coefficients α_{H_2} and α_{O_2} and the exchange current densities i_{H_2} and i_{O_2} at cathode and anode. Finally, the electrolyzer input parameter vector contains the efficiency of the auxiliary electrolyzer components η_{Aux}, and the degradation rates $degR_{\mathrm{El},m}$ of each considered operation mode m which are defined in Sect. 2.2.2. Further input vector for the BESS $\overrightarrow{\boldsymbol{BESS}}$ consist of the roundtrip efficiency η_{BESS}, the $CRate$ as ratio between power and capacity, and the lifetime n_{BESS}. To take site specific conditions into account geodata is provided as vector $\overrightarrow{\boldsymbol{GEO}}$. The shapefile sh_{El} determining the available area on

https://doi.org/10.5194/wes-2026-63
Preprint. Discussion started: 9 April 2026

which the electrolyzer can be placed, pocc the point of common coupling, p_{H_2O} the point of water access, p_{POD} the point of hydrogen demand. Besides these inputs, market data for the design optimization is given with the $\overrightarrow{\boldsymbol{MARKET}^{\mathbf{D}}}$ vector, assuming a constant hydrogen price p_{H_2} and a reference value RV describing the average expected electricity price achieved over the lifetime of the WF. For example in Germany the RV given by the Renewable Energy Sources Act (§ 85a EEG 2023 2026) serves as good approximation. Market data for the operation optimization $\overrightarrow{\boldsymbol{MARKET}^{\mathbf{O}}}$ consist of an annual timeseries in hourly resolution of past day-ahead market prices instead of the RV. Finally, the observation period ObservPeriod as part of $\overrightarrow{\boldsymbol{OP}}$ is used to calculate the mean AHP. Within the design optimization method the design parameters P_{El} and W_{BESS} are iteratively adjusted by the Nelder-Mead algorithm that is further described in Sect. **Fehler! Verweisquelle konnte nicht gefunden werden.** (Lagarias et al. 1998). Within a single iteration the operation of the electrolyzer and BESS is defined using a determined operation strategy as described in Sect. 2.2.1. Subsequently, the degradation of the electrolyzer is evaluated based on the previously determined operation according to the method detailed in Sect. 2.2.2. Based on the information regarding the degradation state of the electrolyzer stacks, the timing for stack replacement is decided as outlined in Sect. 2.2.3. Before the termination criterion for the Nelder–Mead optimization is verified, the electrolyzer efficiency is calculated for each time step as specified in Sect. 2.2.5. This calculation incorporates the cell voltage discussed in Sect. 2.1.1 and accounts for the actual degradation occurring as explained in Sect. 2.1.2. This process yields the AHP, the objective function value and the operational power data per time step for the electrolyzer $P_{EL}(t)$ and for charging and discharging the battery. Additional results are the operation-dependent part of the annual profit (OAP), that consists of revenues from electricity and hydrogen sales, variable water procurement costs, and electrolyzer degradation costs. Finally, the LCOH and the optimal values of the design variables P_{EL} and W_{BESS} are given as output. These optimized design variables serve as input for the operational optimization method described in Sect. 2.3, where the OAP is maximized through MIL optimization. Since this step assumes a linearized part-load efficiency as calculated in Sect. 2.3.1 and neglects the impact of degradation on the electrolyzers efficiency even though the degradation is calculated during the optimization as detailed in Sect. 2.3.2, a further degradation evaluation is performed. This is followed by the determination of the actual electrolyzer efficiency per time step and the resulting hydrogen production. Finally, the objective function value, the operational performance parameters, and the actual OAP after the degradation evaluation are reported.

2.1 Electrolyzer model

This work focuses on PEM technology for electrolyzers, as it offers a wider part-load range and rapid system response times compared to alternative methods. These characteristics make PEM technology superior for coupling with fluctuating renewable energy sources compared to other technologies such as alkaline electrolysis or solid oxide electrolysis (Bockelmann et al. 2024), which is why they are widely used in the literature for HRES. In the following sections the basics for calculating the polarization curve, degradation, and part-load efficiency of an electrolysis cell are presented.

https://doi.org/10.5194/wes-2026-63
Preprint. Discussion started: 9 April 2026

eawe european academy of wind energy
Open Access WIND ENERGY SCIENCE DISCUSSIONS

2.1.1 Cell voltage

The load-dependent efficiency of a PEM electrolysis cell η_{cell} is calculated using the polarization curve as a function of the cell voltage U_{cell}. The polarization curve characterizes the electrochemical behavior of an electrolyzer cell and represents the relationship between the current density i_{cell} and the cell voltage U_{cell} (Buttler and Spliethoff 2018, 2440-54). i_{cell} refers to the current relative to the cell surface area A_{cell}. This paper uses an empirical model of an electrical equivalent circuit by Han et al. (2015) and Abdin et al. (2015), where U_{cell} equals the sum of the Nernst voltage U_{Nernst}, also called open circuit voltage, and the activation overpotential U_{act}, the ohmic loss overpotential U_{ohm}, and the diffusion overpotential U_{diff}, as seen in Eq. (1):

$$U_{\text{cell}} = U_{\text{Nernst}} + U_{\text{act}} + U_{\text{ohm}} + U_{\text{diff}}. \quad (1)$$

The cell voltage under ideal conditions to operate the electrolysis is called the Nernst voltage. It is the theoretical minimum voltage for PEM electrolysis cells when other overpotentials are neglected and can be calculated using equation (2)-(4) (Han et al. 2015):

$$U_{\text{Nernst}} = U_{\text{rev}} + \frac{R \cdot T_{\text{cell}}}{z \cdot F} \cdot \ln\left(\frac{a_{H_2} \cdot \sqrt{a_{O_2}}}{a_{H_2O}} \right), \quad (2)$$

$$U_{rev} = 1.229 - 0.9 \cdot 10^{-3}(T_{cell} - 298\ K), \quad (3)$$

$$a_{H_2} = \frac{p_{\text{H}_2}}{p_0}, a_{O_2} = \frac{p_{\text{O}_2}}{p_0}, \ a_{\text{H}_2\text{O}} = 1, \quad (4)$$

where U_{rev} is the reversible voltage under standard pressure conditions, R the gas constant, T_{cell} the electrolyzer operating temperature, z the number of electron moles participating at the electrolysis reaction, F the Faraday constant, a_{H_2} the ideal gas activity of hydrogen depending on the partial pressure p_{H_2} and the standard atmosphere pressure p_0, a_{O_2} the ideal gas activity of oxygen depending on the partial pressure p_{O_2}, and $a_{\text{H}_2\text{O}}$ the activity of liquid water. The activation overvoltage U_{act} derived from the Butler-Volmer equation (Carmo et al. 2013), must be applied to overcome the activation energy for the electrochemical reactions at the electrodes. Following Eq. (5) U_{act} is the sum of the cathode overpotential $U_{\text{act,cat}}$ and the anode overpotential $U_{\text{act,an}}$:

$$U_{\text{act}} = U_{\text{act,cat}} + U_{\text{act,an}}, \quad (5)$$

with

$$U_{\text{act,cat}} = \frac{R \cdot T_{\text{cell}}}{\alpha_{\text{cat}} \cdot F} \sinh^{-1}\left(\frac{i_{\text{cell}}}{2 \cdot i_{o,\text{cat}}} \right), \quad (6)$$

$$U_{\text{act,an}} = \frac{R \cdot T_{\text{cell}}}{\alpha_{an} \cdot F} \sinh^{-1}\left(\frac{i_{\text{cell}}}{2 \cdot i_{o,\text{an}}} \right), \quad (7)$$

where α_{cat} and α_{an} are the charge transfer coefficients and $i_{\text{o,cat}}$ and $i_{\text{o,an}}$ are the exchange current densities of the cathode respective the anode. U_{ohm} defines the ohmic overpotential caused by the electrolysis cell resistances. According to Ohm's law, it is calculated as the product of the electrical cell resistance R_{cell} and i_{cell}. The cell resistance consists mainly of the resistance of the cell membrane (Abdin et al. 2015), wherefore the resistance of the electrodes and bipolar plates are neglected.

https://doi.org/10.5194/wes-2026-63
Preprint. Discussion started: 9 April 2026

eawe european academy of wind energy
Open Access WIND ENERGY SCIENCE DISCUSSIONS

In this work, U_{ohm} is consequently represented as a function of i_{cell}, the membrane thickness δ_{m}, and the membrane conductivity σ_{m}, as seen in eq. (8).

$$U_{\mathrm{ohm}} = R_{\mathrm{cell}} \cdot A_{\mathrm{cell}} \cdot i_{\mathrm{cell}} = \frac{\delta_{\mathrm{m}}}{\sigma_{\mathrm{m}}} \cdot i_{\mathrm{cell}}, \tag{8}$$

where σ_m is a function of the membrane humidification degree λ and T_{cell}, following Eq. (9):

$$\text{with } \sigma_{\mathrm{m}} = (0.005139 \cdot \lambda - 0.00326) \cdot e^{1268 \cdot (\frac{1}{303} - \frac{1}{T_{\mathrm{cell}}})}. \tag{9}$$

Finally, U_{diff} describes the diffusion overpotential caused by mass transport in the electrolyzer. Studies show that U_{diff} is much lower than U_{ohm} and U_{act} (Hernández-Gómez et al. 2020). For this reason, we follow other studies and assume U_{diff} to be zero (Görgün 2006; Shiva Kumar und Himabindu 2019; García-Valverde et al. 2012).

2.1.2 Degradation

Degradation can be understood as an additional voltage that must be overcome to enable electrolysis, adding an additional coefficient to Eq. (1). Factors influencing degradation include membrane and catalyst properties (Tomić et al. 2023; Buttler und Spliethoff 2018), the operating temperature (Frensch et al. 2019), and the input power of the electrolyzer over time $P_{\mathrm{El}}(t)$. A comprehensive review on the influence and modelling approaches of degradation in PEM electrolyzer is provided by Makhsoos et al. (2025). Due to the high complexity of the different degradation mechanisms, we assume a fixed set of technical properties for the membrane, catalyst, temperature and pressure, while our focus in this work is the relationship between electrolyzer input power and its degradation. This aspect is of particular interest, as the electrolyzer is only powered by a WF, without any connection to the electricity grid. Tully et al. (2023) and so Lu et al. (2023) defining degradation rates for constant operation, fluctuating operation, and start-stop cycles of a PEM electrolyzer. Since the degradation rates from Tully et al. (2023) are experimentally validated, we assume those. We define a constant electrolyzer operation when the load difference for one hour of operation is lower than 3 % of the electrolyzers rated power P_{El}. If the load difference exceeds the limit the electrolyzer is assumed to operate fluctuating.

2.1.3 Efficiency

The efficiency of an electrolysis cell η_{cell} is described by multiplying the voltage efficiency η_V and the Faraday efficiency η_F by the ratio of the produced hydrogen to the input power following Eq. (10).

$$\eta_{\mathrm{cell}} = \eta_V \cdot \eta_F = \frac{\Delta H_{\mathrm{H_2}} \cdot \dot{n}_{\mathrm{H_2}}}{U_{\mathrm{cell}} \cdot i_{\mathrm{cell}} \cdot A_{\mathrm{cell}}}, \tag{10}$$

where $\Delta H_{\mathrm{H_2}}$ is the lower heating value and $\dot{n}_{\mathrm{H_2}}$ the real mass flow of hydrogen. η_V is defined as the ratio between the thermally neutral potential U_{th} and U_{cell}, given in Eq. (11) (Hernández-Gómez et al. 2020).

$$\eta_V = \frac{U_{\mathrm{th}}}{U_{\mathrm{cell}}} \tag{11}$$

η_F reflects losses due to gas diffusion and is correlated to $\dot{n}_{\mathrm{H_2}}$ and the ideal mass flow of hydrogen $\dot{n}_{\mathrm{H_2,ideal}}$, following Eq. (12):

https://doi.org/10.5194/wes-2026-63
Preprint. Discussion started: 9 April 2026

eawe european academy of wind energy
Open Access WIND ENERGY SCIENCE DISCUSSIONS

$$\eta_F = \frac{\dot{n}_{\mathrm{H_2}}}{\dot{n}_{\mathrm{H_2,ideal}}}, \tag{12}$$

with the ideal mass flow calculated by Eq. (13) (Yodwong et al. 2020):

$$\dot{n}_{\mathrm{H_2}} = \frac{i_{\mathrm{cell}} \cdot A_{\mathrm{cell}}}{z \cdot F} \cdot \eta_F. \tag{13}$$

Equation (14) shows the overall efficiency of an electrolyzer η_{El} with multiple cells and stacks and can be calculated by η_{cell} and an additional efficiency for auxiliary structures η_{Aux} such as water and heat management systems (Cheng et al. 2025; Lu et al. 2023; Tofighi-Milani et al. 2025):

$$\eta_{\mathrm{El}} = \eta_{\mathrm{cell}} \cdot \eta_{\mathrm{Aux}} = \frac{\Delta H_{\mathrm{H_2}} \cdot \eta_F}{U_{\mathrm{cell}} \cdot z \cdot F} \cdot \eta_{\mathrm{Aux}}, \tag{14}$$

where η_{cell} is substituted to a combination of Eq. (10) and (13).

2.2 Design optimization

Within the design optimization the optimal rated power of the electrolyzer and the battery capacity are determined to maximize the overall profit over a defined observation period. This problem is formulated as a nonlinear optimization problem (NLP) with two continuous and non-negative decision variables, $P_{\mathrm{El}}^{\mathrm{D}}$ and $W_{\mathrm{BESS}}^{\mathrm{D}}$. It is solved using the Nelder–Mead algorithm, a derivative-free method commonly applied to NLPs (Scholz 2018). The primary objective of design optimization is to maximize the AP of the HWF. The objective function is given in Eq. (15):

$$\max(\mathrm{AP}) = \max\big((\mathrm{AEP} - \mathrm{ECHS}) \cdot (\mathrm{RV} - \mathrm{LCOE}) + \mathrm{AHP} \cdot (p_{\mathrm{hy}} - \mathrm{LCOH})\big), \tag{15}$$

where AEP denotes the annual energy production of the WF and ECHS the total energy consumption of the hydrogen system (Reichartz et al. 2024a). The LCOE represents the average cost per unit of electricity generated by the WF over its lifetime, accounting for capital, operation, and maintenance costs. AHP is the annual hydrogen product that is delivered to the point of hydrogen demand and p_{hy} the assumed hydrogen price. Lastly, the LCOH are calculated according to Eq. (16):

$$\mathrm{LCOH} = \frac{\sum_c (\mathrm{CAPEX}_{y=0,c} + \mathrm{AF}_c \cdot \mathrm{OPEX}_c + \sum_{y=1}^{n} \frac{\mathrm{CAPEX}_{\mathrm{reinvest},c,y}}{(1+i)^y} - \frac{\mathrm{CAPEX}_{\mathrm{rest},c}}{(1+i)^n})}{\sum_{y=1}^{n} \frac{M_{t,\mathrm{H_2}}}{(1+i)^y}}, \tag{16}$$

with the present value annuity factor AF_c following Eq. (17):

$$\mathrm{AF}_c = \frac{(1+i)^{n_c} - 1}{(1+i)^{n_c} \cdot i}. \tag{17}$$

The numerator of Eq. (16) represents the TOTEX of the hydrogen system and the denominator the discounted cumulative hydrogen production over the observation period n, where $M_{\mathrm{t,H_2}}$ denotes the hydrogen mass produced in year t. The parameter n_c specifies the lifetime of component c, and i the applied discount rate. The index c refers to the individual components of the hydrogen system consisting of the electrolyzer, battery, power cable, power converter, water and hydrogen pipeline, utilized water amount, and the hydrogen compressor and storage. Except for the battery these costs are calculated by the method of Reichartz et al. (2024b). $\mathrm{CAPEX}_{y=0,c}$ denotes the initial investment costs, while OPEX_c represents the annual

https://doi.org/10.5194/wes-2026-63
Preprint. Discussion started: 9 April 2026

eawe european academy of wind energy
Open Access WIND ENERGY SCIENCE DISCUSSIONS

operation and maintenance costs, which are annualized using AF_c. Reinvestment costs occurring in year y are given by $CAPEX_{reinvest,c,y}$ and are discounted. The remaining value at the end of n is accounted by the residual cost term $CAPEX_{rest,c}$.

2.2.1 Fixed operation strategy for electrolyzer and BESS

The operation of an electrolyzer and a BESS within a HWF influences the electrolyzers degradation and thus the amount of hydrogen produced. To overcome the complex HFW operation within the design method we define an operating strategy for the electrolyzer and BESS so that as much green hydrogen as possible gets produced. For the electrolyzer that means the strategy prioritizes supplying as much power as possible from the WF to the electrolyzer. This approach ensures a higher capacity factor of the electrolyzer increases hydrogen production and, at constant TOTEX, therefore reduces the LCOH. According to Equation (15), this would in turn lead to increased profit. Even though it is a strong simplification, is has been found to be a useful approach by (Reichartz et al. 2024b). However, when modelling the electrolyzer load-dependent efficiency and degradation, this conclusion is no longer straightforward, as the TOTEX are not constant and hydrogen production is not strictly proportional to the input power. Nevertheless, this strategy is employed to obtain a reasonably solution. The battery is operated in a way that minimizes the number of shut-downs of the electrolyzer, thereby avoiding the high degradation associated with frequent start-stop cycles (Sect. 2.1.2). The power flows in timestep t corresponding to the assumed operating strategy are shown in Figure 2 and described in the following section.

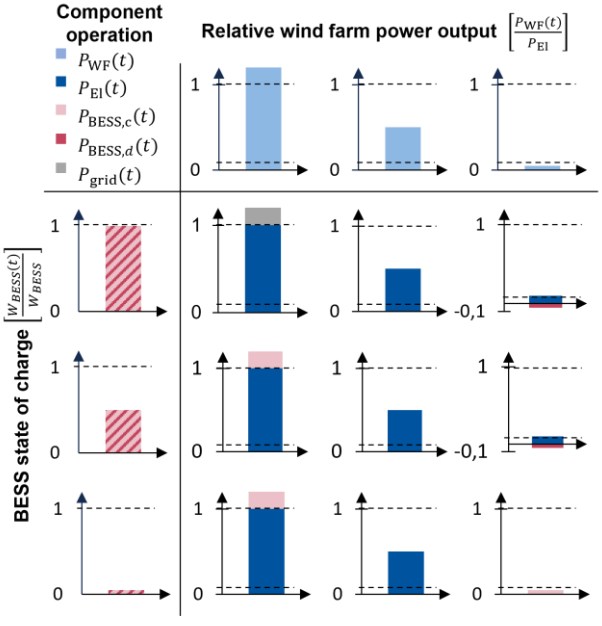

Figure 2: Overview of power flows for timestep in the assumed operation strategy.

The distribution of the WF power among the BESS, the electrolyzer, and the electricity grid, as defined in the assumed operating strategy, depends on both the WF power available at timestep t (top row, Figure 2) and the battery's state of charge at that timestep t (left column, Figure 2). If the available WF power exceeds the nominal power of the electrolyzer

https://doi.org/10.5194/wes-2026-63
Preprint. Discussion started: 9 April 2026

($P_{WF}(t)/P_{El} > 1$), the electrolyzer operates at rated power. Any surplus power is used to charge the BESS. If the BESS is already fully charged, the excess power is fed into the grid. If the WF power is below the nominal electrolyzer power but above the minimum operating threshold (P_{El}^{min}), the entire wind farm power is supplied to the electrolyzer. In the final case, the wind power is insufficient to meet the minimum part-load requirement of the electrolyzer. If the battery has sufficient state of charge to compensate for the deficit relative to the electrolyzers minimum load ($W_{BESS}(t) \geq P_{El}^{min} - P_{WF}(t)$), it is discharged accordingly, thereby preventing a shutdown of the electrolyzer. If that is not the case, the electrolyzer must be shut down. The remaining wind power is then used to charge the battery.

2.2.2 Electrolyzer degradation evaluation

In the literature, degradation studies primarily investigate constant and fluctuating electrolyzer input power as well as start–stop operation (Sect. 2.1.2). Some studies distinguish between steady-state operation at full load, part load and off state. Based on this, the following operating states are defined within our model:

1. Steady-state operation at rated power (rated)
2. Steady-state operation at part-load (partl)
3. Steady-state operation at off-state (off)
4. Fluctuating operation (fluct)
5. Start-stop operation (stop)

Since no universal definitions of these operating states exist, a formal definition of a steady-state operation was introduced in Sect. 2.1.2. Figure 3 shows a flowchart of the degradation evaluation process. For the evaluation of degradation up to timestep t, binary decision variables $b_m(t)$ are introduced for each defined operating mode $m \in \{\text{rated}, \text{partl}, \text{off}, \text{fluct}, \text{stop}\}$. These variables are multiplied by the corresponding degradation rates $degR_{El,m}$ to calculate the cumulative degradation $Deg_{El}(t)$ until t. The degradation associated with a start-stop cycle is added at the time of shutdown.

https://doi.org/10.5194/wes-2026-63
Preprint. Discussion started: 9 April 2026

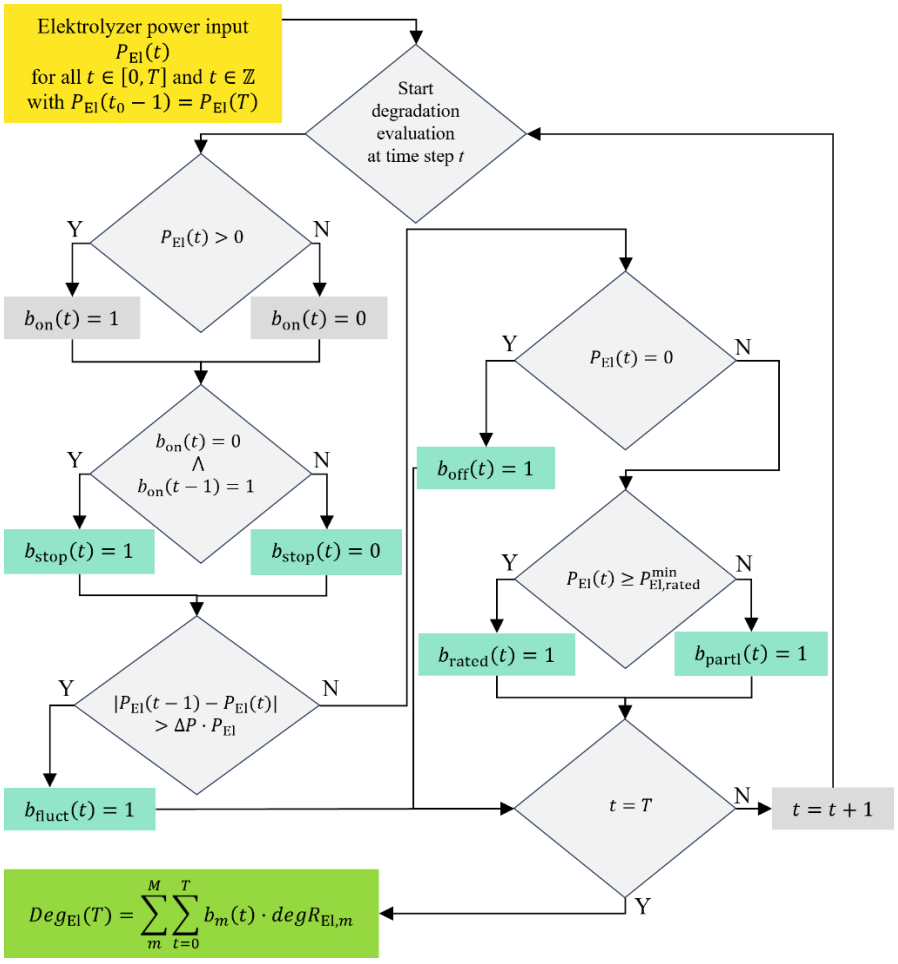

Figure 3: Flowchart to evaluate the operation dependent degradation of an electrolyzer.

Giving the electrolyzers input power $P_{El}(t)$ for each time step, the degradation evaluation loop starts with t equals zero and iteratively increases until t equals T. First, an auxiliary variable $b_{on}(t)$ is introduced to indicate whether the electrolyzer is operating at time t ($b_{on}(t) = 1$) or not ($b_{on}(t) = 0$). Subsequently, it is checked whether the electrolyzer has been switched off at time t, which corresponds to a transition from the on-state at the previous time step t-1 ($b_{on}(t-1) = 1$) to the off-state in t ($b_{on}(t) = 0$). Next, based on the previously defined definition for steady-state operation, it is decided whether the electrolyzer is operating in steady state or fluctuating mode. If the input power is classified as steady, the absolute value of the input power is used to distinguish between constant off-state ($b_{off}(t) = 1,\ if\ P_{El}(t) = 0$), constant full-load operation ($b_{rated}(t) = 1,\ if\ P_{El}(t) > P_{El,rated}^{min}$) and constant part-load operation (($b_{partl}(t) = 1$, otherwise). The operating modes fluct, off, rated, and partl are mutually exclusive. Accordingly, if one binary variable equals one at t, all others are equal to zero at that time. Using this method, the operation-dependent degradation over the entire year can be determined by multiplying the binary variables for each operating mode and timestep with the corresponding degradation rates.

https://doi.org/10.5194/wes-2026-63
Preprint. Discussion started: 9 April 2026

eawe european academy of wind energy
Open Access WIND ENERGY SCIENCE DISCUSSIONS

2.2.3 Electrolyzer stack exchange

The degradation of the electrolyzer stacks might result in a need for replacement over their lifetime. Within the model, a stack replacement resets the degradation state to zero, incurring replacement costs. Other modeling approaches commonly assumed a fixed stack lifetime (Lim et al. 2021) or a replacement criterion based on a predefined efficiency loss of approximately 10 % (Grant et al. 2024; Ibáñez-Rioja et al. 2025). In this study, an alternative and more physically grounded approach is adopted. According to Buttler und Spliethoff (2018) the maximum cell voltage of PEM electrolyzers ranges between 1.65 and 2.5 V at a nominal current density of 2 A cm^{-2}. On this basis, a stack is required to be replaced before the maximum cell voltage of $U_{cell}^{max} = 2.5$ V is exceeded because of degradation-induced overvoltage. Stack replacement is restricted at the end of a year and all stacks within the electrolyzer are operated in the same way. During the optimization of P_{El} and W_{BESS}, the latest technically permissible replacement time is selected. The time of a stack replacement decision $X_{s,y}$ is formulated as a binary decision variable and a constraint is imposed to ensure that the maximum allowable cell voltage is not exceeded. The binary decision variable $X_{s,y}$ is therefore defined for each stack s and indicates whether the stack is replaced at the end of year y or not, following Eq. (18):

$$\mathrm{X_{s,y}} = \begin{cases} 1 & \text{replacement of stack s in } y \\ 0 & \text{otherwise} \end{cases} \quad \forall\, s \in Stacks\,, y \in ObservPeriod. \tag{18}$$

The costs for stack replacements $CAPEX_{SE,y}$ in year y are modelled according to Eq. (19):

$$CAPEX_{SE,y} = \sum_{s=1}^{S} \frac{z_{Stacks} \cdot CAPEX_{El}}{S} \cdot X_{s,y} \tag{19}$$

The parameter z_{Stacks} denotes the share of stack costs relative to the total electrolyzer investment costs $CAPEX_{El}$. According to the International Renewable Energy Agency (IRENA), approximately 45 % of the total system costs are attributed to the stacks, while 55 % relate to balance-of-plant components (IRENA 2020). In general, significant future cost reductions are expected for PEM electrolyzer stacks due to their high cost-reduction potential (Smolinka et al. 2018). For this reason, a reduced cost share of $z_{Stacks} = 40$ % is assumed. $CAPEX_{El}$ describes the specific investment costs of PEM electrolyzers, which are assumed to be 1000 € kW^{-1}. Dividing this value by the number of stacks S that constitute the electrolyzer allows the investment cost of a single stack to be determined. Both the costs of all stack replacements and the resulting reduction in cumulative degradation are accounted for the computation of the AP.

2.2.4 Electrolyzer efficiency and annual hydrogen production

All calculations and formulations required to determine efficiency and degradation have been presented in the previous sections. These elements are consolidated in the following in order to compute the AP. The efficiency of the electrolyzer is calculated based on Equation (14) in Sect. 2.1.3 . In addition to physical constants, the efficiency depends on the cell voltage $U_{cell}(t)$ and the Faraday efficiency $\eta_F(t)$. The cell voltage is linked to the current density i_{cell}, and thus to the electrolyzer input power, through the polarization curve. Furthermore, $U_{cell}(t)$ increases over time due to degradation. The cumulative degradation up to timestep t was described in Sect. 2.2.2. Consequently, the cell voltage is expressed as

https://doi.org/10.5194/wes-2026-63
Preprint. Discussion started: 9 April 2026

eawe european academy of wind energy
Open Access WIND ENERGY SCIENCE DISCUSSIONS

345 $$U_{cell}(t) = f_{polarisation\_curve}(i_{cell}(t)) + Deg_{El}(t). \quad (20)$$

In the case of a stack replacement, the cumulative degradation is reset to zero; otherwise, it increases continuously over the operating period. In addition to the cell voltage, the Faraday efficiency must be determined to calculate the overall efficiency. It is computed according to the model proposed by Yodwong et al. (2020):

$$\eta_F = \left(-0.0034 \cdot p_{H_2} - 0.001711\right) \cdot \frac{A_{cell}}{i_{cell}} + 1 \quad (21)$$

350 where p_{H_2} represents the operating pressure at the cathode of the PEM electrolyzer. This allows the electrolyzer efficiency to be fully determined for each timestep. With this the AHP is obtained by multiplying the electrolyzer input power at each t by the corresponding efficiency and summing over the entire year:

$$AHP = \sum_{t=0}^{8760} P_{El}(t) \cdot \eta_{El}(t) \quad (22)$$

With the AHP, finally, all parameters and variables of Eq. (15) are determined. In the following section a method is presented
355 to verify the assumed operation strategy for the electrolyzer and BESS within the design optimization. This is done by a supplementary MIL operation optimization model using the previous optimized design variables P_{El}^{D} and W_{BESS}^{D} as fixed input parameters.

2.3 Operation optimization

This subsection introduces the mixed-integer linear (MIL) operation optimization of the HWF system over one year with
360 hourly resolution, implemented in the Open Energy Modelling Framework (oemof) (Hilpert et al. 2018; Krien et al. 2020), which we further expanded. As shown in Figure 1 the aim is to maximize the OAP of the previous designed P_{El} and W_{BESS} through optimizing the operation of the electrolyzer and BESS under time-varying electricity prices and WF power generation. Within the operation optimization the electrolyzer part-load efficiency curve calculated based on Sect. 2.2.4 gets linearized according to Sect. 2.3.1. The operation-dependent degradation of the electrolyzer is calculated within the operation
365 optimization following Sect. 2.3.2, but its influence on the efficiency cannot be incorporated since it would introduce non-linearities. Therefore, the actual efficiency losses associated with degradation are neglected during the MIL operation optimization. After the optimization, however, an evaluation following the procedure described in Sect. 2.2.2 is conducted to determine the real degradation, with which the actual electrolyzer efficiency $\eta_{El}^{O}(t)$ at each timestep and the annual hydrogen production AHP^{O} can be calculated. The objective function within the MIL optimization is defined as

370 $$\max(\mathrm{OAP}) = \max\left(\sum_{t=0}^{T}(SE(t) \cdot p_{\mathrm{elec}}(t) + SH(t) \cdot p_{\mathrm{hy}}(t) - WSC(t)) - DegC_{\mathrm{El}}\right), \quad (23)$$

where $SE(t)$ denotes the electricity sold to the day-ahead market at each timestep t, remunerated at the corresponding market price $p_{\mathrm{elec}}(t)$. $SH(t)$ represents the amount of hydrogen sold, valued at the assumed hydrogen price $p_{\mathrm{H_2}}$. $WSC(t)$ accounts for the time-dependent water supply costs associated with hydrogen production and the term $\mathrm{DegC_{El}}$ represents the electrolyzer degradation costs and is calculated as

375 $$\mathrm{DegC_{El}} = \frac{TAD}{U_{cell}^{max} - U_{cell}^{t_0}(\mathrm{i}_{cell}^{max})} \cdot CAPEX_{SE}, \quad (24)$$

https://doi.org/10.5194/wes-2026-63
Preprint. Discussion started: 9 April 2026

where TAD denotes the total annual degradation of the electrolyzer. $U_{\text{cell}}^{\max}$ is the maximum allowable cell voltage, while $U_{\text{cell}}^{t_0}(\mathrm{i}_{\text{cell}}^{\max})$ denotes the cell voltage at nominal current $\mathrm{i}_{\text{cell}}^{\max}$ at the beginning of operation t_0. The parameter $CAPEX_{SE}$ represents the stack exchange costs according to Eq. (19). The OAP monetizes electricity and hydrogen revenues while internalizing water supply and electrolyzer degradation costs, thereby incentivizing profit-maximizing operation that accounts for both immediate market returns and long-term capital preservation.

2.3.1 Linearization of electrolyzer part load efficiency

The part-load efficiency of the electrolyzer can be calculated according to Sect. 2.2.4 and is linearized within the operation optimization. An example of a non-linear and a linearized electrolyzer part-load efficiency and power output over the power input is shown in Figure 4.

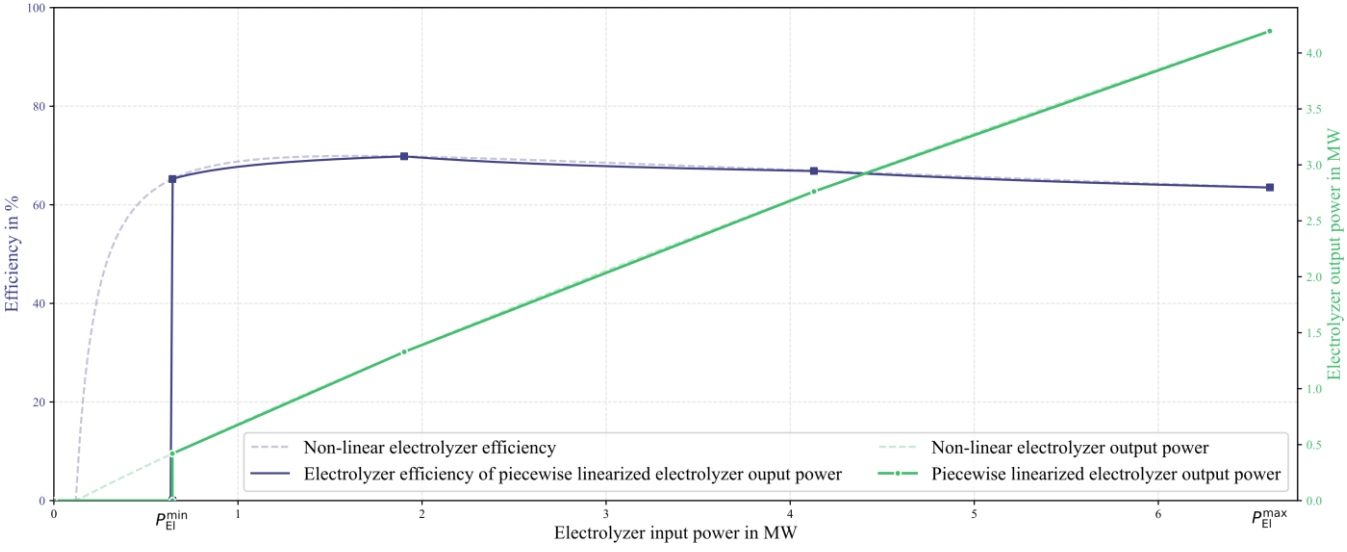

Figure 4: Exemplary illustration of the non-linear and piecewise linearized part-load electrolyzer power output (right axis) and the non-linear part-load efficiency and the efficiency of the linearized output power of an electrolyzer (left axis) in relation to the electrolyzer input power.

Figure 4 illustrates the linearization of the electrolyzer model used in the optimization framework. The primary y-axis (right) depicts the output power as a function of the electrolyzer input power. To accurately represent operational constraints, the model accounts for a minimum load threshold $P_{\text{El}}^{\min}$. Below this point, the system remains in standby mode with zero output, followed by a vertical discontinuity at to reach the physical operating curve. The green segments represent the piecewise linearization, showing a high degree of fit with the non-linear physical reference (dashed green). The secondary y-axis (left) shows the corresponding electrolyzer efficiency. A key feature of this visualization is the actual piecewise efficiency (solid purple line). Unlike a direct linearization of efficiency, this curve is derived from the linearized power segments (dashed green). This results in a hyperbolic efficiency progression within each linear segment, highlighting the model's ability to capture the characteristic part-load efficiency increase while maintaining the linearity required for ML programming. The discrepancy

https://doi.org/10.5194/wes-2026-63
Preprint. Discussion started: 9 April 2026

between the solid and dashed purple lines quantifies the approximation error introduced by the choice of breakpoints. The piecewise linearized part-load input-output relation of the electrolyzer power was implemented in oemof according to Gurobi Optimization (2026).

2.3.2 MIL degradation model

In order to take the operation-dependent degradation of the electrolyzer within the operation optimization into account, the following constraints are integrated into oemof. The TAD is equal to the sum of the annual degradation AD_m of the degradation mode m, as seen in Eq. (25).

$$TAD = \sum_m^M AD_m \quad (25)$$

The same five degradation modes as shown in Sect. 2.2.2 are considered. Following Eq. (26) AD_m is calculated as the sum over all timesteps t until T of the binary variable $b_m(t)$ indicating if m is active at t or inactive, multiplied with its degradation rate $degR_{El,m}$.

$$AD_m = degR_{El,m} \cdot \sum_{t=0}^{T} b_m(t) \quad (26)$$

With Eq. (27) it is ensured that exactly one of each constant modes is active at t:

$$b_{off}(t) + b_{partl}(t) + b_{rated}(t) = 1 \quad (27)$$

Further Eqs. (28) – (32) are needed to determine whether the electrolyzer operates in constant partial load state or at rated power. Therefore, the auxiliary power variables for constant partial load $I_{partl}(t)$ and for constant rated power $I_{rated}(t)$ are introduced. As shown in Eq. (28) the sum of these auxiliary power variables is equal to the electrolyzer input power $P_{El}(t)$:

$$P_{El}(t) = I_{partl}(t) + I_{rated}(t). \quad (28)$$

Equation (29) to (32) identifying at which electrolyzer input power range the constant part-load or the constant rated power mode is active:

$$I_{partl}(t) \geq b_{partl}(t) \cdot P_{El}^{min}, \quad (29)$$

$$I_{partl}(t) \leq b_{partl}(t) \cdot 0.95 * P_{El}, \quad (30)$$

$$I_{rated}(t) \geq b_{rated}(t) \cdot (0.95 * P_{El} + \varepsilon), \quad (31)$$

$$I_{rated}(t) \leq b_{rated}(t) \cdot P_{El}. \quad (32)$$

To prevent equation (30) and (31) both being satisfied at 95 % P_{El}, an ε is introduced that clearly separates the two modes from each other. Besides the constant operation modes, the electrolyzer can be in fluctuation mode if active. To describe this mode the auxiliary variable $ALD(t)$ is needed as the absolute value of the electrolyzer input power difference between two

https://doi.org/10.5194/wes-2026-63
Preprint. Discussion started: 9 April 2026

consecutive timestep. As expressed in Eq. (33) $ALD(t)$ is the sum of the positive load difference $PLD(t)$ and the negative load difference $NLD(t)$:

$$ALD(t) = PLD(t) + NLD(t), \tag{33}$$

whereas $PLD(t)$ and $NLD(t)$ denote the positive and negative components of the load difference. Their definition depends on the rated electrolyzer power P_{El} and the binary variable pos, as expressed in Eq. (34) and (35):

$$PLD(t) \leq P_{El} \cdot pos, \tag{34}$$

$$NLD(t) \leq P_{El} \cdot (1 - pos). \tag{35}$$

pos indicates the sign of the load difference $LD(t)$ and results from subtracting the electrolyzer input power at the previous timestep t-1 from that at timestep t according to Eq. (36), allowing further decomposition into its positive $LD(t)$ and negative parts $NLD(t)$ following Eq. (37):

$$LD(t) = P_{El}(t) - P_{El}(t-1), \tag{36}$$

$$LD(t) = PLD(t) - NLD(t). \tag{37}$$

To determine when the fluctuating mode and therefore the binary variable $b_{fluct}(t)$ is active, $ALD(t)$ is linked to a minimum power threshold ΔP_{El}^{min}, as seen in Eqs. (38) and (39). This ensures that only sufficiently large changes in input power are classified as fluctuations.

$$ALD(t) \geq b_{fluct}(t) \cdot \Delta P_{El}^{min} \tag{38}$$

$$ALD(t) \leq b_{fluct}(t) \cdot P_{El} + \Delta P_{El}^{min} \tag{39}$$

The stop mode is governed by constraints expressed in Eqs. (40) – (41), which ensure that transitions to the turned-off state are correctly detected and represented within the model:

$$b_{stop}(t) \geq b_{off}(t) - b_{off}(t-1) \ , \tag{40}$$

$$b_{stop}(t) \leq b_{off}(t-1), \tag{41}$$

$$b_{stop}(t) \leq 1 - b_{off}(t), \tag{42}$$

where the binary variable $b_{stop}(t)$ can be described by equations that only depend on the constant off binary variable at different timesteps. At each timestep, it must be guaranteed that the electrolyzer operates either in a constant or a fluctuating mode; this coupling of corresponding binary variables is established using Eqs. (43) and (44).

$$b_{fluct}(t) + b_{const.}(t) = 1 \tag{43}$$

$$b_{off,c}(t) + b_{partl,c}(t) + b_{rated,c}(t) = b_{const}(t) \tag{44}$$

https://doi.org/10.5194/wes-2026-63
Preprint. Discussion started: 9 April 2026

Distinguishing among constant operating modes requires additional auxiliary variables, introduced as shown in Eqs. (45) - (47), to ensure an unambiguous assignment to each respective state.

$$b_{partl,c}(t) \leq b_{partl}(t) \quad (45)$$

$$b_{partl,c}(t) \leq b_{const}(t) \quad (46)$$

$$b_{partl,c}(t) \geq b_{partl}(t) + b_{const}(t) - 1 \quad (47)$$

Finally, further constraints given in Eqs. (48) - (50) ensure correct identification of operation at rated power within the set of constant modes.

$$b_{rated,c}(t) \leq b_{rated}(t) \quad (48)$$

$$b_{rated,c}(t) \leq b_{const}(t) \quad (49)$$

$$b_{rated,c}(t) \geq b_{rated}(t) + b_{const}(t) - 1 \quad (50)$$

3 Model application and results

In this section the methodology outlined in Sect. 2 is applied to a case study of an existing WF in Germany. The use case and the assumed input parameters are defined in Sect. 3.1. Section 3.2 presents the results of the design optimization for maximizing the AP of the HWF and the influence of the added electrolyzer model and a BESS. Finally, Sect. 3.3 provides a comparative analysis between the operating strategy of the design optimization and the results of the operation optimization described in Sect. 2.3 and the subsequent degradation evaluation of Sect. 2.2.2.

3.1 Use case

The existing WF “Rhede (Ems)” with 21 turbines and a rated power of 67.55 MW (windpark-rhede 2025), located in North-West of Germany is considered. The WF area, the distance to the point of common coupling, the water supply point, the location of the electrolyzer, a part of the planed German hydrogen grid (Bundesnetzagentur - Hydrogen core network 2026), and the assumed wind rose taken from the New European Wind Atlas (2026) at the center of the wind farm site at 100 m height above the ground level are shown in Figure 5.

https://doi.org/10.5194/wes-2026-63
Preprint. Discussion started: 9 April 2026

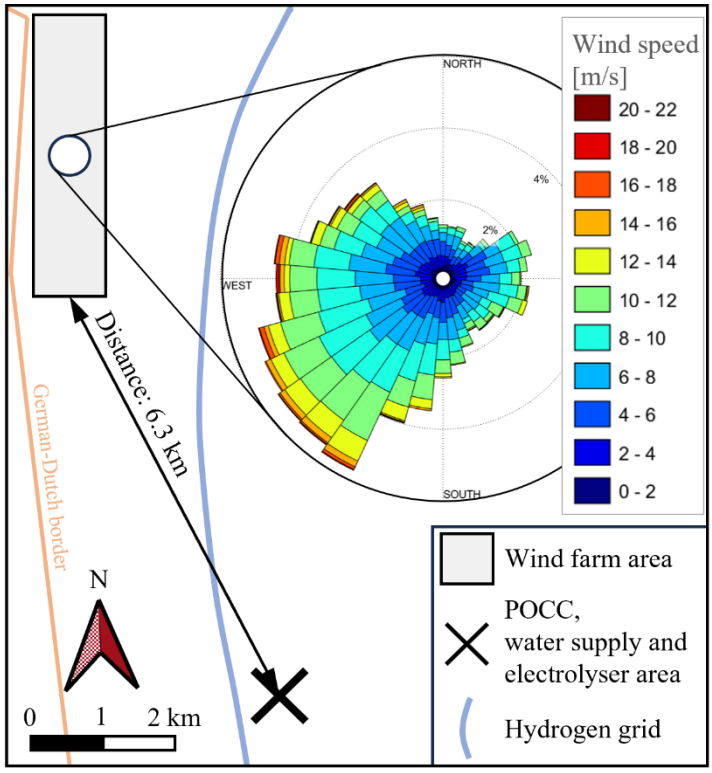

Figure 5: Schematic illustration of the wind farm site and its distance to the POCC, the water supply and the location of the electrolyzer. Also shown is a part of the planned German hydrogen grid and the wind rose at the center of the wind farm site at 100 m height above ground level.

The closest distance between the assumed hydrogen grid and the location of the electrolyzer is 0.61 km. Additionally a factor to transfer the direct distance to a more realistic distance of 1.4 is assumed (Reuß 2019). Since focus of this work are the systems components and their model and operation we do not consider multiple distribution modes. Consequently, we assume that produced hydrogen will be compressed and delivered to the hydrogen grid via pipeline. For a more detailed understanding of the distribution options, the subcomponents available in the model, and the cost functions assumed in this work, please refer to Reichartz et al. (2024b). For the BESS we assume a lifetime of 30 years (Ibáñez-Rioja et al. 2025), CAPEX of 612 \$ kWh^{-1} according to Cole et al. (2025) with an exchange rate for 2024 of 0.92 € $\$^{-1}$ (OECD Economic Surveys: European Union and Euro Area 2025 2025) to 560 € kWh^{-1}, and OPEX of 1% CAPEX per year. Assumed technical design optimization parameters for the input vectors of Figure 1 are listed in Table 1 with their corresponding values and sources.

https://doi.org/10.5194/wes-2026-63
Preprint. Discussion started: 9 April 2026

eawe european academy of wind energy
Open Access WIND ENERGY SCIENCE DISCUSSIONS

Table 1: Input vectors with assumed parameters for the design optimization.

Vector	Parameter	Value	Unit	Source
$\overrightarrow{WF}$	Levelized Cost Of Electricity: LCOE	55.2	€ MWh^{-1}	Own calculations based on
	Wind farm power output: $P_{WF}(t)$	Time series	MW	Roscher (2020)
$\overrightarrow{EL}$	Minimum rated power: $P_{El,rated}^{min}$	0.95 P_{El}	-	-
	Rated stack power: P_{Stack}	1.25	MW	Nel (2025), Bosch (2025)
	Minimum relative partial load: P_{Stack}^{min}	0.10 P_{Stack}	-	Nel (2025), Bosch (2025)
	Maximum current density: i_{cell}^{max}	2	A cm^{-2}	Buttler und Spliethoff (2018)
	Maximum cell voltage: U_{cell}^{max}	2.5	V	Buttler und Spliethoff (2018)
	Cell area: A_{cell}	0.095	m^2	Buttler und Spliethoff (2018)
	Operating temperature: t_{El}	80	°C	Han et al. (2015)
	Operating pressure cathode: p_{H_2}	13.78	bar	Han et al. (2015)
	Operating pressure anode: p_{O_2}	1.013	bar	Han et al. (2015)
	Transfer coefficient cathode: α_{H_2}	0.5	-	Han et al. (2015)
	Transfer coefficient anode: α_{O_2}	2.0	-	Han et al. (2015)
	Exchange current density cathod: i_{H_2}	0.1	A cm^{-2}	Abdin et al. (2015)
	Exchange current density anode: i_{O_2}	10^{-7}	A cm^{-2}	Abdin et al. (2015)
	Efficiency of subcomponents: η_{Aux}	0.90	-	Cheng et al. (2025)
	Degradation rates for each operation mode: $degR_{El,m}$	rated: 3 partl: 3 off: 3 fluct: 23.9 stop: 237	µV h^{-1}	Tully et al. (2023)
$\overrightarrow{BESS}$	Roundtrip efficiency: η_{BESS}	0.95	-	Kurzweil und Dietlmeier (2018)
	C-rate: CRate	1	h^{-1}	-
$\overrightarrow{GEO}$	Shapefiles and points determining sh_{El}, pocc, p_{H2O}, p_{POD}	-	-	-
$\overrightarrow{MARKET_D}$	Hydrogen price: p_{hy}	7.8	€ kg^{-1}	Based on mean price of (EEX 2026)
	Electricity reference value: RV	73.5	€ MWh^{-1}	(EEG2023Bundesamt für Justiz; § 85a EEG 2023 2026; Bockelmann et al. 2024)
$\overrightarrow{OP}$	ObservPeriod	25	years	-

https://doi.org/10.5194/wes-2026-63
Preprint. Discussion started: 9 April 2026

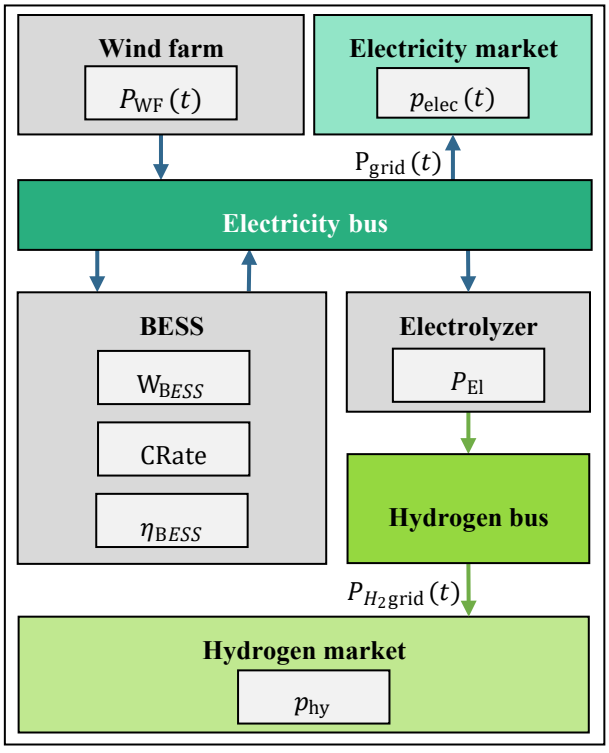

Figure 6.

Figure 6: Schematic overview of the modelled energy system for the operation optimization in oemof.

The power generated by the WF at a timestep $P_{WF}(t)$ is fed into an electricity bus. At the electricity bus the sum of all in- and outgoing flows must be zero for all t. The electricity bus is connected to a battery with a fixed capacity C_{BESS}, a C-rate CRate, and an overall storage efficiency η_{BESS}. Electricity can be sold at the electricity market or fed into the electrolyzer with a fixed rated power P_{El}. The time varying electricity price $p_{elec}(t)$ consist of hourly day-ahead market data from Germany in 2024 (Energy-Charts 2026). The produced hydrogen can be sold to the hydrogen market for a fixed hydrogen price p_{hy} of 7.8 € kg^{-1} equals , which was the average price for hydrogen in 2024 of the HYDRIX (eex 2024).

3.2 Design optimization

This section presents the results of the design optimization method introduced in Sect. 2.2, applied to the case study described in the previous Sect. 3.1, noting that the operational optimization of Sect. 2.3 has not been performed at this stage. Due to the described model of the electrolyzer efficiency, degradation, stack replacement, and degradation evaluation, the design optimization problem is nonlinear. In the context of nonlinear and non-convex optimization, it is generally only possible to identify local optima. Demonstrating that the global optimum has been found is considerably more challenging (Kallrath 2013).

https://doi.org/10.5194/wes-2026-63
Preprint. Discussion started: 9 April 2026

eawe european academy of wind energy
Open Access WIND ENERGY SCIENCE DISCUSSIONS

However, to identify the region where the global optimum likely resides, the design space is explored by varying the design variables P_{El} and W_{BESS}. Therefore, the ratio of the electrolyzer rated power to the WF rated power is varied from 0.015 to 1.0 and the BESS capacity from 0.0 to 1.0 in 0.015 increments. Thus, an increment corresponds to a deviation of 1 MW respectively 1 MWh. The central panel of Fig.

Figure 7 shows the AP for the parameter space with the hydrogen price assumed in the use case described in Sect. 3.1. The left and right heat maps of Fig.

Figure 7 are also showing the AP for deviating hydrogen prices.

Figure 7: Annual profit as function of electrolyzer rated power and rated BESS capacity over wind farm rated power for three different hydrogen prices.

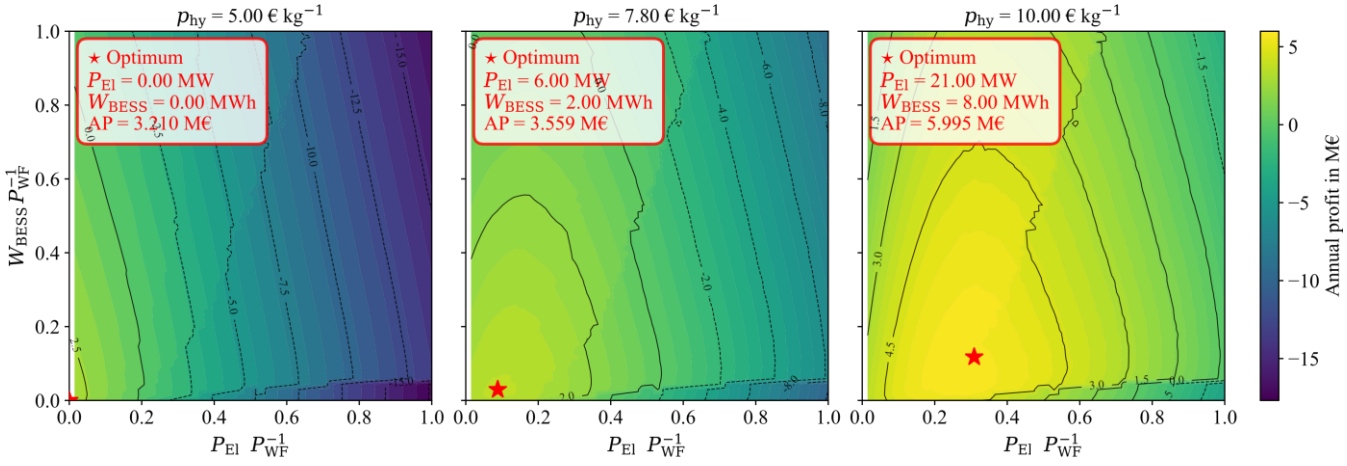

Figure 7 illustrates the strong dependence of the optimal HWF design on the assumed hydrogen price. The results indicate that the global optimum shifts toward larger electrolyzer and BESS capacities as the hydrogen price increases. With a constant hydrogen price of 5.0 € kg^{-1}, the maximum AP occurs for the stand-alone WF. This AP without electrolyzer and BESS is calculated as the product of AEP and the difference between the RV and the LCOE amounting to 3.21 M€ a^{-1}. A threshold price of 7.0 € kg^{-1} is required for a configuration with 1 MW and 0 MWh to achieve a higher AP than the stand-alone WF. Below this hydrogen price level, the implementation of a HWF does not yield economic benefits under the given assumptions. As seen in the middle and right panels of Figure 7 the hydrogen price of 7.8 € kg^{-1}, results in an optimal configuration shift to 6 MW and 2 MWh, while at 10 € kg^{-1} it further increases to 21 MW and 8 MWh. The results indicate that variations in the electrolyzer rated power have more significant impact on the AP than variations in the BESS capacity. The optimum identified in the central panel of

Figure 7 with p_{hy} equals 7.8 € kg^{-1} serves as the initial configuration for the design optimization method, which employs the Nelder-Mead algorithm described in Sect. 2.2 for the given use case of Sect. 3.1. The optimized design variables, as well as the mean AP, mean annual revenues, mean AHP, and TOTEX determined over the observation period, are detailed in Table 2.

https://doi.org/10.5194/wes-2026-63
Preprint. Discussion started: 9 April 2026

Table 2: Design optimization results of the described use case over the entire observation period.

Output	Value	Unit
Optimized electrolyzer rated power	6.435	MW
Optimized BESS capacity	2.034	MWh
Mean AP	3.57	M€ a^{-1}
Mean annual hydrogen profit	1.12	M€ a^{-1}
Mean annual electricity profit	2.45	M€ a^{-1}
Mean AHP	626	t a^{-1}
Mean annual hydrogen revenue	4.88	M€ a^{-1}
Mean annual electricity revenue	9.84	M€ a^{-1}
LCOH	6.01	€ $kg_{H_2}{}^{-1}$
TOTEX without WF	44.20	M€
TOTEX electrolyzer	40.00	M€
TOTEX pipeline system incl. water supply	1.56	M€
TOTEX electricity supply	1.37	M€
TOTEX BESS	1.27	M€

The optimized design variables obtained are an electrolyzer rated power of 6.435 MW and a BESS capacity of 2.034 MWh. The AP of 3.57 M€ a^{-1} of the HWF is composed of the annual electricity profit by a share of approximately two-third and the annual hydrogen profit by one-third. For the given hydrogen price, the AP of the HWF is about 11 % above the AP of the stand-alone WF, demonstrating that the HWF can have a significant impact on the economics of the system installed at the given WF site. The annual electricity revenue accounts for 9.84 M€ a^{-1}, representing approximately two thirds of the total revenues, while hydrogen sales contribute the remaining one third with 4.88 M€ a^{-1}, which is consistent with the relative contributions to the AP. The TOTEX without the existing WF respectively of the added hydrogen system amount to 44.20 M€ over the entire observation period. The largest share of TOTEX is associated with the electrolyzer, driven primarily by variable electrolyzer OPEX in the form of electricity procurement costs, which account for about 64 % of the electrolyzer TOTEX. The remaining costs are significantly lower. This cost distribution emphasizes that the profit optimization of the HWF depends primarily on the electricity procurement and secondary on the electrolyzer investment costs, rather than on the cost reduction of peripheral components.

To assess the impact of the modified electrolyzer modelling and the inclusion of a BESS by avoiding the strong price sensitivity the LCOH of the method of Reichartz et al. (2024b) is compared with the LCOH obtained in this study, accounting for the

https://doi.org/10.5194/wes-2026-63
Preprint. Discussion started: 9 April 2026

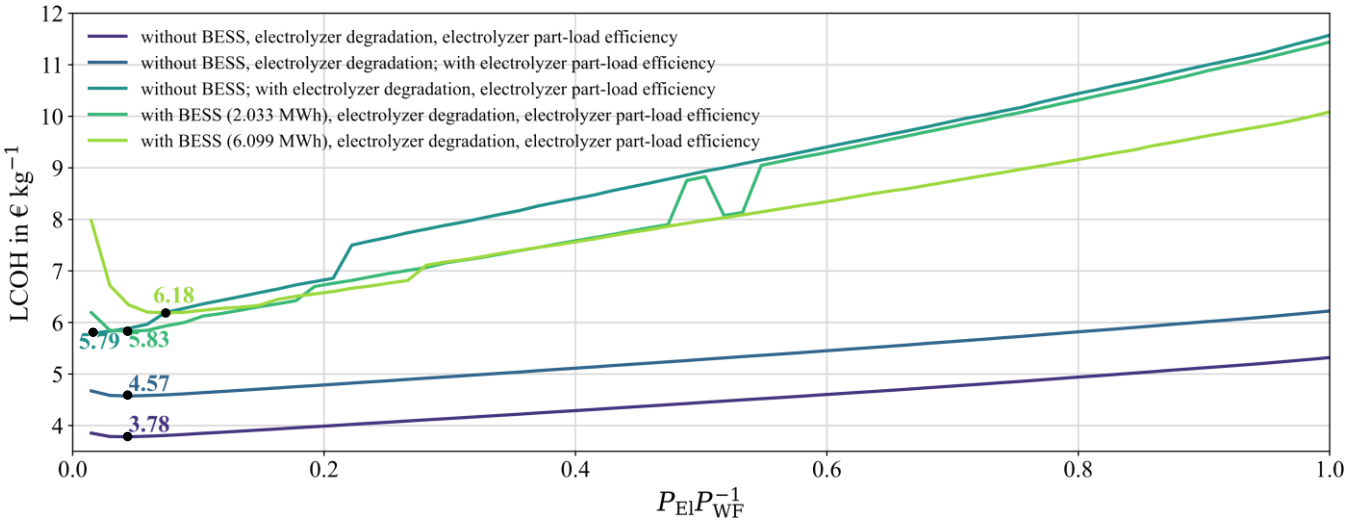

Figure 8: LCOH over the ratio of electrolyzer rated power to wind farm rated power for four different modelling approaches and two different BESS sizes.

A comparison of the minimum LCOH values of the model variants without BESS shows that neglecting electrolyzer degradation leads to an underestimation of the LCOH by approximately 21 %, while neglecting both degradation and partial-load efficiency results in an underestimation of about 35 %. These results highlight the critical importance of accurately representing both degradation effects and part-load efficiency in electrolyzer modelling. Adding a BESS capacity of 2.033 MWh, that was previously identified as optimum for the AP maximization for the given use case, actually leads to an increase in LCOH by less than one percent while increasing the AP by 5 % in this scenario. While the incremental hydrogen yield is insufficient to offset the additional BESS-related TOTEX, resulting in a marginal LCOH increase, the system benefits from enhanced operational flexibility. Consequently, the BESS effectively increases the AP by capturing higher market revenues that outweigh the rise in levelized production costs. An increased BESS capacity shifts the LCOH minimum to higher electrolyzer capacities while further increasing LCOH. Ultimately, these findings underscore that the choice of the objective function is pivotal for the optimal sizing of both the electrolyzer and the BESS, as it fundamentally dictates whether the integration of a BESS is perceived as a profit benefit or a cost driver.

A technical driver behind this economic trade-off is the BESS ability to mitigate electrolyzer degradation. Specifically, the operation strategy assumed in Sect. 2.2.1 results in an annual electrolyzer degradation, calculated according to Sect. 2.2.2, for the in Sect. 3.1 presented HWF system of $0.1138\ \mathrm{V\ a^{-1}}$. This TAD corresponds to degradation costs of $0.586\ \mathrm{M€\ a^{-1}}$, when converted according to Eq. (24). If the BESS is removed, the TAD increases to $0.1577\ \mathrm{V\ a^{-1}}$, increasing the degradation cost

https://doi.org/10.5194/wes-2026-63
Preprint. Discussion started: 9 April 2026

by 0.226 M€ a^{-1}. The electrolyzer degradation with and without BESS divides into the different operation modes according to Table 3.

Table 3: Share of the total annual degradation depending on the electrolyzer operation modes with and without BESS.

Operation mode	With BESS: TAD = 0.1138 V a^{-1}		Without BESS: TAD = 0.1577 V a^{-1}	
	AD in V a^{-1}	AD share of TAD in %	AD in V a^{-1}	AD share of TAD in %
rated	0.0145	12.74	0.0145	9.20
partl	0.0019	1.66	0.0008	0.54
off	0.0015	1.35	0.0025	1.61
fluct	0.0665	58.43	0.0668	42.38
stop	0.0294	25.82	0.0730	46.28

The fluctuating operation mode is the dominant driver of electrolyzer degradation in the system with BESS. However, removing the BESS leads to a significant increase in the TAD by more than a third. This is primarily driven by the degradation from start-stop cycles, which more than doubles from 0.0294 V a^{-1} to 0.0730 V a^{-1}. Furthermore, the AP of the System without BESS decreases to 3.4 M€, representing a 4.7 % reduction compared to the configuration featuring a 2.034 MWh BESS. These findings underline the effectiveness of the BESS within the implemented operation strategy by buffering volatile WF power. The battery prevents frequent shutdowns and ensures a more continuous hydrogen production, thereby substantially mitigating cycle-induced degradation of the electrolyzer. While the BESS integration entails additional CAPEX, these costs are offset over the system's operational period by reduced electrolyzer degradation costs and increased hydrogen revenues, even when limited to a buffering operation strategy.

3.3 MIL operation optimization

As described in Section 1, the design and operation of electrolyzers are inherently interdependent. In the design optimization method presented in this study, an operational strategy for the electrolyzer and the BESS is assumed following Section 2.2.2. This assumption is evaluated in this Section by comparing the electrolyzer and BESS operation obtained from the design optimization with the results of the MIL operation optimization introduced in Sect. 2.3 and a subsequent degradation evaluation of Sect. 2.2.2. Figure 9 presents the OAP and its decomposition into annual electricity and hydrogen revenues as well as water supply and degradation costs for both optimization approaches of the first year for operation under constant and variable electricity prices.

https://doi.org/10.5194/wes-2026-63
Preprint. Discussion started: 9 April 2026

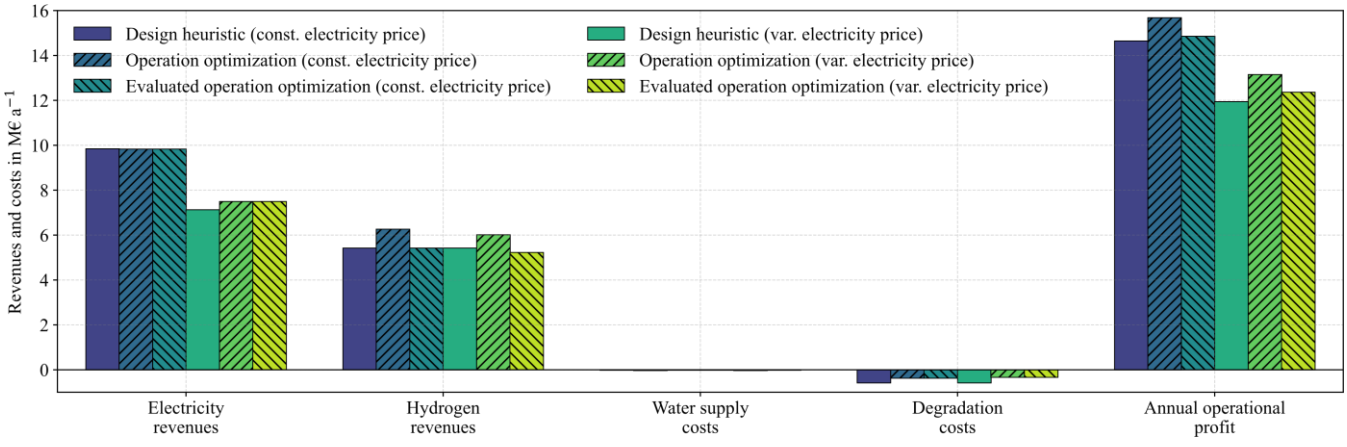

Figure 9: Comparison of the annual operational profit and its shares of the design optimization, the MIL operation optimization, and its degradation evaluation for constant and variable electricity prices.

Figure 9 show that the assumed constant electricity price in the design optimization leads to a systematic overestimation of electricity revenues and, consequently, of the OAP by 23 % when compared to variable electricity price conditions of 2024. This highlights the limitations of design-stage economic assumptions when applied to real-world market environments with pronounced price volatility. In addition, the degradation costs associated with the operating strategy assumed during the design optimization amount to 0.59 M€ $a^{-1}$and can be reduced by about 44 % through the proposed operational optimisation under variable price conditions. This reduction underlines the strong influence of operational control on component ageing and long-term economic performance.

Neglecting degradation-induced efficiency losses and using a piecewise linearized efficiency of the electrolyzer within the operation optimization leads to an overestimation of hydrogen revenues by 15 % under variable electricity price conditions, relative to the revenues obtained from the subsequent degradation evaluation. Initially, the MIL operation optimization suggests a significant economic potential, with a projected OAP approximately 10 % higher than that of the design heuristic. Despite the subsequent revenue correction due to degradation effects and efficiency linearization, the evaluated OAP remains above the value calculated in the design phase, reaching 104 % under variable electricity prices and 101 % under constant electricity prices. This demonstrates that MIL operational optimization, even when neglecting degradation-related efficiency losses, can slightly enhance economic performance relative to the simplified operation assumptions in the design optimization. However, the gap between the initial 10 % projection and the evaluated 1 % to 4 % gain highlights the clear potential for further improvements through a more comprehensive representation of degradation effects within the economically optimum operation of the HWF.

To analyse the impact of the assumed hydrogen price on the optimal HWF operation and to evaluate the discrepancies between the system components operation of the design optimization and the MIL operation optimization, Figure 10 presents different

https://doi.org/10.5194/wes-2026-63
Preprint. Discussion started: 9 April 2026

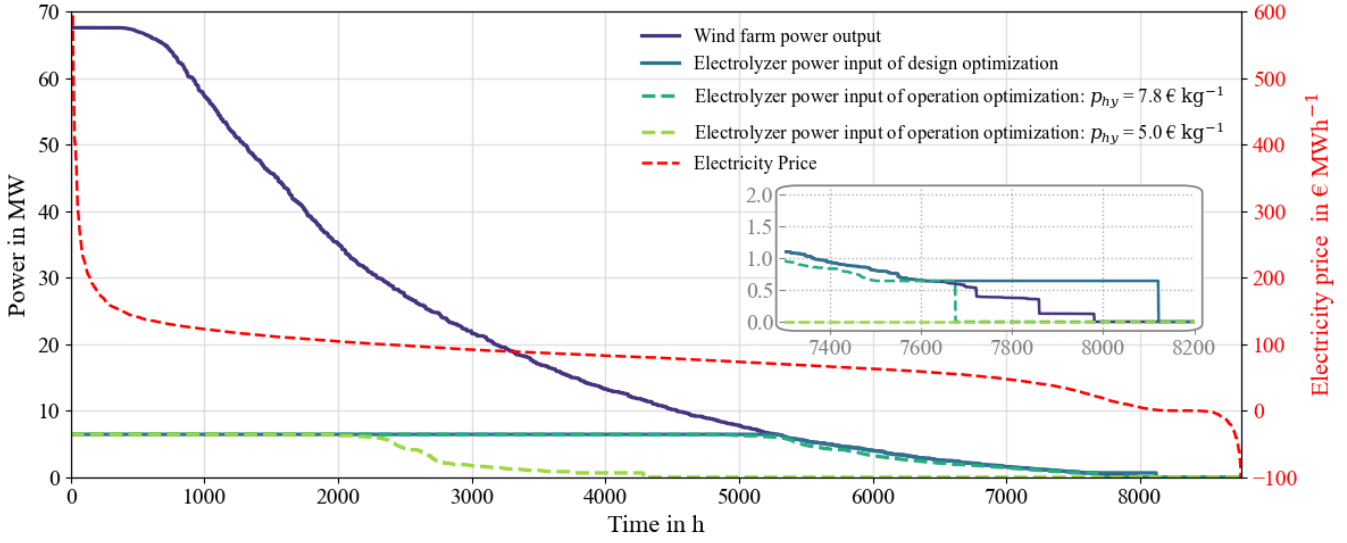

Figure 10: Sorted load duration curves of the WF power output, the electrolyzer power input of the design optimization, and for the MIL operation optimization for two different hydrogen price scenarios, and the sorted electricity price over one year.

The comparative analysis of the sorted load duration curves, as illustrated in Figure 10, reveals that the operational characteristics of the design heuristic and the operational optimization differ only marginally at a hydrogen price of 7.8 € kg^{-1}. Specifically, the design heuristic (dark blue line) accounts for 6,418 full load hours (FLH) per year, while the operational optimization (teal solid line) reaches 6,213 FLH. This high degree of similarity is primarily attributed to the fact that the assumed hydrogen price is significantly higher than the average electricity day-ahead market price of 79.6 € MWh^{-1}. Under these conditions, the marginal revenue from hydrogen production mostly exceeds the opportunity costs of direct electricity sales, incentivizing the system to maximize hydrogen output regardless of the specific operation approach. Even when reducing the hydrogen price to 5.0 € kg^{-1} (light green dashed line), which triggers a shift in the optimized electrolyzer operation to 2,858 FLH, the economic performance of the design heuristic remains competitive. Despite its price-independent nature and the resulting inability to account for fluctuating market signals, the annual operational profit achieved through MIL optimization exceeds that of the static design optimization operation by only 4.5 %. This suggests that while the heuristic remains active during periods where market electricity prices exceed the marginal revenue of hydrogen production, the associated economic losses are largely mitigated by the overall system design. Although the operation optimization selectively decreases the input power of the electrolyzer during high-price electricity periods, the marginal profit gain remains limited. It must be noted, however, that the high accuracy of the operation heuristic within the design optimization observed here is specific to the investigated use case.

https://doi.org/10.5194/wes-2026-63
Preprint. Discussion started: 9 April 2026

eawe european academy of wind energy
Open Access WIND ENERGY SCIENCE DISCUSSIONS

4 Discussion and future work

4.1 Design optimization methodology advancements

This study extends the optimization framework for co-located wind-hydrogen systems developed by Reichartz et al. (2024a). A significant advancement is the integration of an empirical electrolyzer model from Han et al. (2015) and Abdin et al. (2015) that calculates electrolyzer efficiency as a function of cell voltage and Faraday efficiency. Degradation of the electrolyzer depending on five different operating modes was added as by increasing the electrolyzer cell voltage and therefore decreasing efficiency. To reduce these electrolyzer degradation a BESS operating as an electricity buffer is added into the HWF. The objective function was shifted from LCOH to AP allowing a more comprehensive economic assessment. By integrating revenue structures for both hydrogen and electricity sales, it was demonstrated that approximately two-thirds of the total AP is generated through electricity revenues, while one-third stems from hydrogen sales. Electricity procurement costs were identified as the primary driver of the hydrogen system's TOTEX, aligning with results reported by Nachit et al. (2026). Despite these operational costs, the HWF configuration demonstrates clear economic advantages under the assumed energy prices. Specifically, the AP of a stand-alone WF is approximately 10 % lower than that of the optimal HWF investigated in this use case. This margin underscores the potential of hybridization to enhance the economic efficiency of a given WF site. Consequently, these findings are of particular relevance for WF operators and project planners aiming to evaluate the viability of extending existing or planned WFs with decentralized PEM electrolysis and BESS. By providing a methodology that balances capital investment against operational flexibility and component degradation, the method enables a risk-adjusted assessment of integrated energy systems by keeping site specific costs into account. In this context, the design optimization identified a global optimum for the electrolyzer rated power and BESS capacity of the investigated use case. This optimum electrolyzer rated power was found to be close to 10 % power relative to the installed WF power, that is also within the optimum range of electrolyzer power found by Chatzistlyianos et al. (2025).

To evaluate the operation and the resulting revenues within the design methodology, a fixed operation strategy for the electrolyzer and the BESS was developed. This strategy prioritizes maximizing the AHP to effectively reduce the LCOH using WF power exclusively, while minimizing degradation intense start-stop cycles by the BESS. By mapping electrolyzer degradation across five distinct operational modes, this study introduces a method to evaluate cumulative annual degradation. The results underscore that degradation leads to a 21 % underestimation of the LCOH, which increases to 35 % when part-load efficiency is also ignored. For project planners, these findings are crucial to avoid overly optimistic economic forecasts. Furthermore, the results show that while a BESS can reduce the annual degradation by more than a third it leads to an increase in LCOH, highlighting that the choice of the objective function exerts a profound influence on the optimal HWF design and underscores the necessity of precise BESS dimensioning. While the BESS effectively protects the electrolyzer stack from premature aging, the BESS itself is subject to wear-and-tear through cycling (Xu et al. 2018). BESS degradation, however, was neglected in this study, likely leading to an underestimation of the LCOH. This may obscure a trend observed by

https://doi.org/10.5194/wes-2026-63
Preprint. Discussion started: 9 April 2026

Chatzistlyianos et al. (2025), where BESS integration consistently increases the LCOH. Furthermore, this study assumes a pure buffering strategy for the BESS. In reality, multi-market BESS can generate significant additional value through revenue stacking, such as participating in frequency regulation or energy arbitrage (Mohamed et al. 2023). While such strategies could enhance the overall economic performance of the HWF, they would also increase battery cycling and further complicate the operational dispatch. Including these multi-market opportunities alongside BESS degradation costs would likely shift the optimum economical BESS capacity and require further operation strategies to balance the trade-off between electrolyzer protection and battery health.

4.2 Operation strategy comparison

To demonstrate the profit potential of the assumed operation strategy in the design optimization method, a MIL operation optimization was performed for the designed system. This comparative approach is particularly valuable for system analysts and project developers, as it quantifies the performance gap between simplified heuristic dispatch and mathematically optimal operation. By maximizing the operation-dependent profit under variable market prices conditions over one year, a profit increase to 110 % was identified. However, the MIL operation optimization uses a piecewise linearization of the part-load efficiency and neglects the direct impact of degradation on the electrolyzers efficiency during the decision-making process. A subsequent evaluation of the operation optimization results, which factored these effects back in, showed that the actual profit gain was reduced to 104 % relative to the design optimization OAP. This profit discrepancy highlights that idealized optimization results must be critically verified against physical degradation models to establish realistic business cases and avoid overestimating long-term revenues. To refine these results, a MIL rolling-horizon optimization approach like the one from Chen et al. (2024) could present a viable solution to incorporate these degradation-related efficiency losses in shorter intervals. This would allow the operational strategy to adapt to the aging of the electrolyzer stacks more realistic. Alternatively, nonlinear optimization could directly integrate degradation effects into the decision-making process, although this significantly increases computational effort and may hinder the identification of a global optimum. Implementing more sophisticated allocation approaches, such as rotating or daisy-chain stack usage, could further mitigate degradation and enhance revenues (Zhou et al. 2025; Cheng et al. 2025). However, such refinements would simultaneously increase the model complexity and the associated computational burden. Additionally, this work did not explore variations in electricity price profiles or wind generation time series, both of which can exert a substantial influence on optimal operating behaviour. In markets with high price volatility or different meteorological characteristics, the divergence between static rules and adaptive optimization might increase significantly, potentially limiting the transferability of these findings. To derive reliable investment decisions, a hybrid wind farm design must demonstrate robustness against external factors. Therefore, the integrate of adaptive operational optimization directly into the sizing process can ensure that the system responds to market volatility or volatile wind power generation, providing a robust basis for identifying the optimal HWF design even under uncertain external conditions.

https://doi.org/10.5194/wes-2026-63
Preprint. Discussion started: 9 April 2026

eawe european academy of wind energy
Open Access WIND ENERGY SCIENCE DISCUSSIONS

Code and data availability

No data other than that given in the paper are required to produce the presented results. The source code is not published.

Author contributions

The concept and method of the present study were developed by DF, TR, and LB. DF and TR performed the initial implementation of the software, which was extended and improved by TP. DF and TP performed the initial text creation. TR, TR, MK, and GJ were responsible for supervision, revision, and final approval. All authors have read and agreed to the published version of the paper.

Competing interests

The contact author has declared that none of the authors has any competing interests.

Disclaimer

Copernicus Publications remains neutral with regard to jurisdictional claims made in the text, published maps, institutional affiliations, or any other geographical representation in this paper. While Copernicus Publications makes every effort to include appropriate place names, the final responsibility lies with the authors. Views expressed in the text are those of the authors and do not necessarily reflect the views of the publisher.

Acknowledgements

AI was used to assist with language and phrasing for some text parts of the manuscript.

Financial support

This open-access publication was funded by the RWTH Aachen University.

Review statement

https://doi.org/10.5194/wes-2026-63
Preprint. Discussion started: 9 April 2026

References

§ 85a EEG 2023 (2026). Online verfügbar unter https://www.gesetze-im-internet.de/eeg_2014/__85a.html, zuletzt aktualisiert am 16.01.2026, zuletzt geprüft am 16.01.2026.

Abdin, Z.; Webb, C. J.; Gray, E.MacA. (2015): Modelling and simulation of a proton exchange membrane (PEM) electrolyser cell. In: *International Journal of Hydrogen Energy* 40 (39), S. 13243–13257. DOI: 10.1016/j.ijhydene.2015.07.129.

Balderrama, Sergio; Lombardi, Francesco; Riva, Fabio; Canedo, Walter; Colombo, Emanuela; Quoilin, Sylvain (2019): A two-stage linear programming optimization framework for isolated hybrid microgrids in a rural context: The case study of the "El Espino" community. In: *Energy* 188, S. 116073. DOI: 10.1016/j.energy.2019.116073.

Bechmann, A.; Quick, J. (2025): Market-Driven Wind Resource Assessment. In: *J. Phys.: Conf. Ser.* 3025 (1), S. 12001. DOI: 10.1088/1742-6596/3025/1/012001.

Bockelmann, Marina; Becker, Maik; Stypka, Sebastian; Bauer, Stina; Minke, Christine; Turek, Thomas (2024): Erzeugung von Wasserstoff durch Elektrolyse. In: *Chemie in nserer Zeit* 58 (1), S. 29–45. DOI: 10.1002/ciuz.202300024.

Bosch (2025): Hybrion PEM-Elektrolysis Stack. Online verfügbar unter https://www.bosch-hydrogen-energy.com/media/pem_electrolysis/hybrion_pem_electrolysis_stacks/bosch-hybrion-pem-electrolysis-stacks-specification-sheet.pdf, zuletzt geprüft am 12.2025.

Bošnjaković, Mladen; Katinić, Marko; Santa, Robert; Marić, Dejan (2022): Wind Turbine Technology Trends. In: *Applied Sciences* 12 (17), S. 8653. DOI: 10.3390/app12178653.

Bundesamt für Justiz: Erneuerbare-Energien-Gesetz. EEG 2023. Fundstelle: §85a. Online verfügbar unter https://www.gesetze-im-internet.de/eeg_2014/__85a.html.

Bundesnetzagentur - Hydrogen core network (2026). Online verfügbar unter https://www.bundesnetzagentur.de/EN/Areas/Energy/HydrogenCoreNetwork/start.html, zuletzt aktualisiert am 15.01.2026, zuletzt geprüft am 15.01.2026.

Buttler, Alexander; Spliethoff, Hartmut (2018): Current status of water electrolysis for energy storage, grid balancing and sector coupling via power-to-gas and power-to-liquids: A review. In: *Renewable and Sustainable Energy Reviews* 82, S. 2440–2454. DOI: 10.1016/j.rser.2017.09.003.

Canbulat, Seda; Balci, Kutlu; Canbulat, Onder; Bayram, I. Safak (2021): Techno-Economic Analysis of On-Site Energy Storage Units to Mitigate Wind Energy Curtailment: A Case Study in Scotland. In: *Energies* 14 (6), S. 1691. DOI: 10.3390/en14061691.

Carmo, Marcelo; Fritz, David L.; Mergel, Jürgen; Stolten, Detlef (2013): A comprehensive review on PEM water electrolysis. In: *International Journal of Hydrogen Energy* 38 (12), S. 4901–4934. DOI: 10.1016/j.ijhydene.2013.01.151.

Chatzistlyianos, Evangelos; Psarros, Georgios; Chinaris, Periklis; Papathanassiou, Stavros (2025): Cost Estimation for Green Hydrogen Production and Distribution. In: 2025 21st International Conference on the European Energy Market (EEM). 2025

https://doi.org/10.5194/wes-2026-63
Preprint. Discussion started: 9 April 2026

21st International Conference on the European Energy Market (EEM). Lisbon, Portugal, 27.05.2025 - 29.05.2025: IEEE, S. 1–6.

Chen, Ruochen; Gao, Ciwei; Ming, Hao (2024): Rolling-horizon optimization strategy for wind-storage system in electricity market. In: *IET Renewable Power Gen* 18 (5), S. 825–836. DOI: 10.1049/rpg2.12954.

Cheng, Kangle; He, Shan; Hu, Bing (2025): Power adaptive control strategy for multi-stack PEM photovoltaic hydrogen systems considering electrolysis unit efficiency and hydrogen production rate. In: *Sustainable Energy Technologies and Assessments* 75, S. 104200. DOI: 10.1016/j.seta.2025.104200.

Cole, Wesley; Vignesh Ramasamy; and Merve Turan (2025): Cost Projections for Utility-Scale Battery Storage: 2025 Update. Hg. v. National Renewable Energy Laboratory. Golden, CO 80401 (NREL/TP-6A40-93281). Online verfügbar unter https://docs.nrel.gov/docs/fy25osti/93281.pdf.

Cozzolino, Raffaello; Bella, Gino (2024): A review of electrolyzer-based systems providing grid ancillary services: current status, market, challenges and future directions. In: *Front. Energy Res.* 12, Artikel 1358333. DOI: 10.3389/fenrg.2024.1358333.

Dolatabadi, A.; Ebadi, R.; Mohammadi-Ivatloo, B. (2019): A Two-Stage Stochastic Programming Model for the Optimal Sizing of Hybrid PV/diesel/battery in Hybrid Electric Ship System. In: *Journal of Operation and Automation in Power Engineering*, S. 16–26. DOI: 10.22098/joape.2019.4395.1349.

eex (2024): HYDRIX. Online verfügbar unter https://www.eex.com/en/markets/hydrogen, zuletzt geprüft am 12.2025.

EEX. Hydrogen (2026). Online verfügbar unter https://www.eex.com/en/markets/hydrogen, zuletzt aktualisiert am 16.01.2026, zuletzt geprüft am 16.01.2026.

Energy-Charts (2026): Spot Market Prices. Fraunhofer ISE. Online verfügbar unter https://www.energy-charts.info/charts/price_spot_market/chart.htm?l=en&c=DE&interval=year&year=2024&minuteInterval=60min&legendItems=ey5, zuletzt aktualisiert am 15.01.2026, zuletzt geprüft am 16.01.2026.

European Comission (2026): Renewable energy targets. Online verfügbar unter https://energy.ec.europa.eu/topics/renewable-energy/renewable-energy-directive-targets-and-rules/renewable-energy-targets_en, zuletzt aktualisiert am 06.03.2026, zuletzt geprüft am 06.03.2026.

European Parliament and Council 2021: REGULATION (EU) 2021/1119 OF THE EUROPEAN PARLIAMENT AND OF THE COUNCIL of 30 June 2021 establishing the framework for achieving climate neutrality and amending Regulations (EC) No 401/2009 and (EU) 2018/1999 (‘European Climate Law’). European Climate Law (Reg. (EU) 2021/1119). Online verfügbar unter http://data.europa.eu/eli/reg/2021/1119/oj, zuletzt geprüft am 06.03.2026.

Fabianek, Paul; Madlener, Reinhard (2024): Techno-economic analysis and optimal sizing of hybrid PV-wind systems for hydrogen production by PEM electrolysis in California and Northern Germany. In: *International Journal of Hydrogen Energy* 67, S. 1157–1172. DOI: 10.1016/j.ijhydene.2023.11.196.

https://doi.org/10.5194/wes-2026-63
Preprint. Discussion started: 9 April 2026

Frensch, Steffen Henrik; Fouda-Onana, Frédéric; Serre, Guillaume; Thoby, Dominique; Araya, Samuel Simon; Kær, Søren Knudsen (2019): Influence of the operation mode on PEM water electrolysis degradation. In: *International Journal of Hydrogen Energy* 44 (57), S. 29889–29898. DOI: 10.1016/j.ijhydene.2019.09.169.

García-Valverde, R.; Espinosa, N.; Urbina, A. (2012): Simple PEM water electrolyser model and experimental validation. In: *International Journal of Hydrogen Energy* 37 (2), S. 1927–1938. DOI: 10.1016/j.ijhydene.2011.09.027.

Görgün, H. (2006): Dynamic modelling of a proton exchange membrane (PEM) electrolyzer. In: *International Journal of Hydrogen Energy* 31 (1), S. 29–38. DOI: 10.1016/j.ijhydene.2005.04.001.

Grant, E.; Brunik, K.; King, J.; Clark, C. E. (2024): Hybrid power plant design for low-carbon hydrogen in the United States. In: *J. Phys.: Conf. Ser.* 2767 (8), S. 82019. DOI: 10.1088/1742-6596/2767/8/082019.

Gurobi Optimization (2026): Nonlinear Constraints - Gurobi Optimizer Reference Manual. Online verfügbar unter https://docs.gurobi.com/projects/optimizer/en/current/features/nonlinear.html#subsubsectiongenconstrfunctionpwl, zuletzt aktualisiert am 23.01.2026, zuletzt geprüft am 02.02.2026.

Han, Bo; Steen, Stuart M.; Mo, Jingke; Zhang, Feng-Yuan (2015): Electrochemical performance modeling of a proton exchange membrane electrolyzer cell for hydrogen energy. In: *International Journal of Hydrogen Energy* 40 (22), S. 7006–7016. DOI: 10.1016/j.ijhydene.2015.03.164.

Hernández-Gómez, Ángel; Ramirez, Victor; Guilbert, Damien (2020): Investigation of PEM electrolyzer modeling: Electrical domain, efficiency, and specific energy consumption. In: *International Journal of Hydrogen Energy* 45 (29), S. 14625–14639. DOI: 10.1016/j.ijhydene.2020.03.195.

Hilpert, S.; Kaldemeyer, C.; Krien, U.; Günther, S.; Wingenbach, C.; Plessmann, G. (2018): The Open Energy Modelling Framework (oemof) - A new approach to facilitate open science in energy system modelling. In: *Energy Strategy Reviews* 22, S. 16–25. DOI: 10.1016/j.esr.2018.07.001.

Hofrichter, Andreas; Rank, Daniel; Heberl, Michael; Sterner, Michael (2023): Determination of the optimal power ratio between electrolysis and renewable energy to investigate the effects on the hydrogen production costs. In: *International Journal of Hydrogen Energy* 48 (5), S. 1651–1663. DOI: 10.1016/j.ijhydene.2022.09.263.

Ibáñez-Rioja, Alejandro; Puranen, Pietari; Järvinen, Lauri; Kosonen, Antti; Ruuskanen, Vesa; Hynynen, Katja et al. (2025): Baseload hydrogen supply from an off-grid solar PV–wind power–battery–water electrolyzer plant. In: *Energy* 322, S. 135304. DOI: 10.1016/j.energy.2025.135304.

IRENA (2020): Green hydrogen cost reduction. Online verfügbar unter https://h2.pe/uploads/IRENA_Green_hydrogen_cost_2020.pdf.

IRENA (2024): Renewable power generation costs in 2023. Hg. v. International Renewable Energy Agency. Abu Dhabi. Online verfügbar unter https://www.irena.org/Publications/2024/Sep/Renewable-Power-Generation-Costs-in-2023, zuletzt geprüft am 06.03.2026.

Kallrath, Josef (2013): Gemischt-ganzzahlige Optimierung: Modellierung in der Praxis. Wiesbaden: Springer Fachmedien Wiesbaden.

https://doi.org/10.5194/wes-2026-63
Preprint. Discussion started: 9 April 2026

Kansara, Rushit; Roldán Serrano, María Isabel (2024): Coupled Design and Operation Optimization for Decarbonization of Industrial Energy Systems Using an Open-Source In-House Tool. In: *Eng* 5 (4), S. 3033–3048. DOI: 10.3390/eng5040158.

Krien, Uwe; Schönfeldt, Patrik; Launer, Jann; Hilpert, Simon; Kaldemeyer, Cord; Pleßmann, Guido (2020): oemof.solph—A model generator for linear and mixed-integer linear optimisation of energy systems. In: *Software Impacts* 6, S. 100028. DOI: 10.1016/j.simpa.2020.100028.

Kurzweil, Peter; Dietlmeier, Otto K. (2018): Elektrochemische Speicher. Wiesbaden: Springer Fachmedien Wiesbaden.

Lagarias, Jeffrey C.; Reeds, James A.; Wright, Margaret H.; Wright, Paul E. (1998): Convergence Properties of the Nelder--Mead Simplex Method in Low Dimensions. In: *SIAM J. Optim.* 9 (1), S. 112–147. DOI: 10.1137/S1052623496303470.

Lim, Dongjun; Lee, Boreum; Lee, Hyunjun; Byun, Manhee; Cho, Hyun-Seok; Cho, Wonchul et al. (2021): Impact of voltage degradation in water electrolyzers on sustainability of synthetic natural gas production: Energy, economic, and environmental analysis. In: *Energy Conversion and Management* 245, S. 114516. DOI: 10.1016/j.enconman.2021.114516.

Lu, Xinyu; Du, Banghua; Zhou, Shenpei; Zhu, Wenchao; Li, Yang; Yang, Yang et al. (2023): Optimization of power allocation for wind-hydrogen system multi-stack PEM water electrolyzer considering degradation conditions. In: *International Journal of Hydrogen Energy* 48 (15), S. 5850–5872. DOI: 10.1016/j.ijhydene.2022.11.092.

Makhsoos, Ashkan; Kandidayeni, Mohsen; Pollet, Bruno G.; Boulon, Loïc (2025): Proton exchange membrane water electrolyzers degradation models review: implications for power allocation and energy management. In: *Journal of Power Sources* 655, S. 238003. DOI: 10.1016/j.jpowsour.2025.238003.

Mohamed, Ahmed; Rigo-Mariani, Rémy; Debusschere, Vincent; Pin, Lionel (2023): Stacked revenues for energy storage participating in energy and reserve markets with an optimal frequency regulation modeling. In: *Applied Energy* 350, S. 121721. DOI: 10.1016/j.apenergy.2023.121721.

Nachit, Ibrahim; Naanani, Hassan; Ikharrazne, Lmokhtar (2026): Dynamic and techno-economic assessment of electrolyser technologies under intermittent renewable energy: Performance and cost competitiveness across six countries. In: *International Journal of Hydrogen Energy* 201, S. 152841. DOI: 10.1016/j.ijhydene.2025.152841.

Nel (2025): PEM Electrolyser - PEM Series. Online verfügbar unter https://nelhydrogen.com/product/psm-series-electrolyser/.

New European Wind Atlas (2026): Welcome to the New European Wind Atlas. Online verfügbar unter https://map.neweuropeanwindatlas.eu/, zuletzt aktualisiert am 15.01.2026, zuletzt geprüft am 15.01.2026.

OECD Economic Surveys: European Union and Euro Area 2025 (2025): OECD Publishing (2025).

Papakonstantinou, Georgios; Algara-Siller, Gerardo; Teschner, Detre; Vidaković-Koch, Tanja; Schlögl, Robert; Sundmacher, Kai (2020): Degradation study of a proton exchange membrane water electrolyzer under dynamic operation conditions. In: *Applied Energy* 280, S. 115911. DOI: 10.1016/j.apenergy.2020.115911.

Peng, Jing; Vijayshankar, Sanjana; King, Jennifer; Mathieu, Johanna (2025): Trade-offs between Battery Energy Storage and Hydrogen Storage in Off-Grid Green Hydrogen Systems. In: Tung Bui (Hg.): Proceedings of the 57th Hawaii International

https://doi.org/10.5194/wes-2026-63
Preprint. Discussion started: 9 April 2026

Conference on System Sciences. Hawaii International Conference on System Sciences: Hawaii International Conference on System Sciences (Proceedings of the Annual Hawaii International Conference on System Sciences).

Reichartz, Thorsten; Jacobs, Georg; Blickwedel, Lucas; Frings, Dustin; Schelenz, Ralf (2024a): Co-Design of a Wind–Hydrogen System: The Effect of Varying Wind Turbine Types on Techno-Economic Parameters. In: *Energies* 17 (18), S. 4710. DOI: 10.3390/en17184710.

Reichartz, Thorsten; Jacobs, Georg; Rathmes, Tom; Blickwedel, Lucas; Schelenz, Ralf (2024b): Optimal position and distribution mode for on-site hydrogen electrolyzers in onshore wind farms for a minimal levelized cost of hydrogen (LCoH). In: *Wind Energ. Sci.* 9 (1), S. 281–295. DOI: 10.5194/wes-9-281-2024.

Reuß, Markus Eduard (2019): Techno-ökonomische Analyse alternativer Wasserstoffinfrastruktur. Dissertation.

Robinius, Martin; Otto, Alexander; Heuser, Philipp; Welder, Lara; Syranidis, Konstantinos; Ryberg, David et al. (2017): Linking the Power and Transport Sectors—Part 1: The Principle of Sector Coupling. In: *Energies* 10 (7), S. 956. DOI: 10.3390/en10070956.

Roscher, Björn (2020): Multi-dimensional wind farm optimization in the concept phase. RWTH Aachen University.

Rozzi, Elena; Grimaldi, Alberto; Minuto, Francesco D.; Lanzini, Andrea (2025): Model complexity and optimization trade-offs in the design and scheduling of hybrid hydrogen-battery systems. In: *Energy Conversion and Management* 344, S. 120306. DOI: 10.1016/j.enconman.2025.120306.

Sayed-Ahmed, H.; Toldy, Á.I.; Santasalo-Aarnio, A. (2024): Dynamic operation of proton exchange membrane electrolyzers—Critical review. In: *Renewable and Sustainable Energy Reviews* 189, S. 113883. DOI: 10.1016/j.rser.2023.113883.

Schnuelle, Christian; Wassermann, Timo; Fuhrlaender, David; Zondervan, Edwin (2020): Dynamic hydrogen production from PV & wind direct electricity supply – Modeling and techno-economic assessment. In: *International Journal of Hydrogen Energy* 45 (55), S. 29938–29952. DOI: 10.1016/j.ijhydene.2020.08.044.

Scholz, Daniel (2018): Optimierung interaktiv. Grundlagen verstehen, Modelle erforschen und Verfahren anwenden. Berlin, Germany, Heidelberg: Springer Spektrum (Lehrbuch).

Shams, Mohammad H.; Niaz, Haider; Na, Jonggeol; Anvari-Moghaddam, Amjad; Liu, J. Jay (2021): Machine learning-based utilization of renewable power curtailments under uncertainty by planning of hydrogen systems and battery storages. In: *Journal of Energy Storage* 41, S. 103010. DOI: 10.1016/j.est.2021.103010.

Shiva Kumar, S.; Himabindu, V. (2019): Hydrogen production by PEM water electrolysis – A review. In: *Materials Science for Energy Technologies* 2 (3), S. 442–454. DOI: 10.1016/j.mset.2019.03.002.

Smolinka, Tom; Wiebe, Nikolai; Sterchele, Philip; Palzer, Andreas; Lehner, Franz; Jansen, Malte et al. (2018): Die zentralen Fragen dieser durch das Bundesministerium für Verkehr und digitale Infrastruktur beauftragten Studie sind, wie sichergestellt werden kann, dass die Wasserelektrolyse zukünftig als leistungsfähige Technologie verfügbar sein wird, und welche Herausforderungen beim Aufbau einer Gigawatt-Elektrolyseindustrie in Deutschland bestehen. Hg. v. Fraunhofer

https://doi.org/10.5194/wes-2026-63
Preprint. Discussion started: 9 April 2026

IPA. Online verfügbar unter https://www.ipa.fraunhofer.de/de/Publikationen/studien/studie-industrialisierung-wasserelektrolyse.html, zuletzt aktualisiert am 20.01.2026, zuletzt geprüft am 20.01.2026.

Tezer, Tuba (2025): Multi-objective optimization of hybrid renewable energy systems with green hydrogen integration and hybrid storage strategies. In: *International Journal of Hydrogen Energy* 142, S. 1249–1271. DOI: 10.1016/j.ijhydene.2025.03.006.

Tofighi-Milani, Mahyar; Fattaheian-Dehkordi, Sajjad; Lehtonen, Matti (2025): Electrolysers: A Review on Trends, Electrical Modeling, and Their Dynamic Responses. In: *IEEE Access* 13, S. 39870–39885. DOI: 10.1109/ACCESS.2025.3546546.

Tomić, Andrej Zvonimir; Pivac, Ivan; Barbir, Frano (2023): A review of testing procedures for proton exchange membrane electrolyzer degradation. In: *Journal of Power Sources* 557, S. 232569. DOI: 10.1016/j.jpowsour.2022.232569.

Tully, Zachary; Starke, Genevieve; Johnson, Kathryn; King, Jennifer (2023): An Investigation of Heuristic Control Strategies for Multi-Electrolyzer Wind-Hydrogen Systems Considering Degradation. In: 2023 IEEE Conference on Control Technology and Applications (CCTA). 2023 IEEE Conference on Control Technology and Applications (CCTA). Bridgetown, Barbados, 16.08.2023 - 18.08.2023: IEEE, S. 817–822.

van Phan, Long; Nguyen-Dinh, Nghia Phu; Nguyen, Khai Manh; Nguyen-Duc, Tuyen (2024): Advanced frequency control schemes and technical analysis for large-scale PEM and Alkaline electrolyzer plants in renewable-based power systems. In: *International Journal of Hydrogen Energy* 89, S. 1354–1367. DOI: 10.1016/j.ijhydene.2024.09.360.

windpark-rhede (2025): Windpark Rhede GmbH & Co. KG. Online verfügbar unter https://windpark-rhede.de/, zuletzt aktualisiert am 12.11.2025, zuletzt geprüft am 15.01.2026.

Xu, Bolun; Oudalov, Alexandre; Ulbig, Andreas; Andersson, Goran; Kirschen, Daniel S. (2018): Modeling of Lithium-Ion Battery Degradation for Cell Life Assessment. In: *IEEE Trans. Smart Grid* 9 (2), S. 1131–1140. DOI: 10.1109/TSG.2016.2578950.

Yodwong, Burin; Guilbert, Damien; Phattanasak, Matheepot; Kaewmanee, Wattana; Hinaje, Melika; Vitale, Gianpaolo (2020): Faraday's Efficiency Modeling of a Proton Exchange Membrane Electrolyzer Based on Experimental Data. In: *Energies* 13 (18), S. 4792. DOI: 10.3390/en13184792.

Zheng, Yi; Huang, Chunjun; Tan, Jin; You, Shi; Zong, Yi; Træholt, Chresten (2023): Off-grid wind/hydrogen systems with multi-electrolyzers: Optimized operational strategies. In: *Energy Conversion and Management* 295, S. 117622. DOI: 10.1016/j.enconman.2023.117622.

Zheng, Yi; You, Shi; Bindner, Henrik W.; Münster, Marie (2022): Incorporating optimal operation strategies into investment planning for wind/electrolyser system. In: *CSEE JPES*. DOI: 10.17775/CSEEJPES.2021.04240.

Zhou, Zelong; Zheng, Menglian; Dong, Binqi; Li, Jiarui (2025): Cluster allocation strategy of multi-electrolyzers in wind-hydrogen system considering electrolyzer degradation under fluctuating operating conditions. In: *Renewable Energy* 242, S. 122381. DOI: 10.1016/j.renene.2025.122381.